

1 **Evaluation of the Community Multiscale Air Quality (CMAQ)**
2 **model v5.0 against size-resolved measurements of inorganic**
3 **particle composition across sites in North America**

4
5 **C. G. Nolte¹, K. W. Appel¹, J. T. Kelly², P. V. Bhave³, K. M. Fahey¹,**
6 **J. L. Collett, Jr.⁴, L. Zhang⁵, and J. O. Young¹**

7 [1]{Atmospheric Modeling and Analysis Division, National Exposure Research Laboratory,
8 Office of Research and Development, U.S. Environmental Protection Agency, Research Triangle
9 Park, North Carolina, USA}

10 [2]{Air Quality Assessment Division, Office of Air Quality Planning and Standards, Office of
11 Air and Radiation, U.S. Environmental Protection Agency, Research Triangle Park, North
12 Carolina, USA}

13 [3]{International Centre for Integrated Mountain Development, Kathmandu, Khumaltar,
14 Lalitpur, Nepal}

15 [4]{Department of Atmospheric Science, Colorado State University, Fort Collins, Colorado,
16 USA}

17 [5]{Air Quality Research Division, Science and Technology Branch, Environment Canada,
18 Toronto, Ontario, Canada}

19 Correspondence to: C. G. Nolte (nolte.chris@epa.gov)

20
21 **Abstract**

22 This work evaluates particle size-composition distributions simulated by the Community
23 Multiscale Air Quality (CMAQ) model using Micro-Orifice Uniform Deposit Impactor (MOUDI)
24 measurements at 18 sites across North America. Size-resolved measurements of particulate SO_4^{2-}
25 , NO_3^- , NH_4^+ , Na^+ , Cl^- , Mg^{2+} , Ca^{2+} and K^+ are compared to CMAQ model output for discrete
26 sampling periods between 2002 and 2005. The observation sites were predominantly in remote
27 areas (e.g. National Parks) in the United States and Canada, and measurements were typically
28 made for a period of roughly one month. For SO_4^{2-} and NH_4^+ , model performance was consistent

1 across the U.S. and Canadian sites, with the model slightly overestimating the peak particle
2 diameter and underestimating the peak particle concentration compared to the observations. Na^+
3 and Mg^{2+} size distributions were generally well represented at coastal sites, indicating reasonable
4 simulation of emissions from sea spray. CMAQ is able to simulate the displacement of Cl^- in aged
5 sea spray aerosol, though the extent of Cl^- depletion relative to Na^+ is often underpredicted. The
6 model performance for NO_3^- exhibited much more site-to-site variability than that of SO_4^{2-} and
7 NH_4^+ , with the model ranging from an underestimation to overestimation of both the peak diameter
8 and peak particle concentration across the sites. Computing $\text{PM}_{2.5}$ from the modeled size
9 distribution parameters rather than by summing the masses in the Aitken and accumulation modes
10 resulted in differences in daily averages of up to $1 \mu\text{g m}^{-3}$ (10%), while the difference in seasonal
11 and annual model performance compared to observations from the IMPROVE, CSN and AQS
12 networks was very small. Two updates to the CMAQ aerosol model—changes to the assumed
13 size and mode width of emitted particles and the implementation of gravitational settling—resulted
14 in small improvements in modeled size distributions.

15

16 **1 Introduction**

17 A detailed understanding of the size, chemical composition, and atmospheric concentration of
18 particulate matter (PM) is needed to assess its effects on human health, visibility, ecosystems, and
19 climate. Assessments of these various PM effects are typically done with mathematical models,
20 and our confidence in the models is established through rigorous evaluation against ambient
21 measurements. The mass concentration, size distribution, and bulk chemical composition of
22 atmospheric PM are most often measured separately, and models are typically evaluated against
23 these independent measures (e.g., Simon et al., 2012). However, it is well established that the PM
24 composition varies considerably with particle size, and these size-resolved chemical characteristics
25 govern the optical and radiative properties of PM. Because the aerodynamic behavior of PM is
26 also a strong function of particle size, the size distributions of different chemical components also
27 influence the human health and environmental effects of PM by affecting where particles deposit
28 in the respiratory tract (Asgharian et al., 2001) or whether they are transported to sensitive
29 ecosystems (Scheffe et al, 2014).

1 Inertial cascade impactors are the most robust devices for collecting size-resolved ambient
2 particles and analyzing their chemical composition (e.g., Marple et al., 1991). Because operating
3 a cascade impactor is labor-intensive and costly, their use has been restricted historically to field
4 studies at individual locations or multi-site campaigns within small geographic regions (e.g., John
5 et al., 1990). Previously, size-composition distributions simulated by the Community Multiscale
6 Air Quality (CMAQ) model were evaluated against Micro-Orifice Uniform Deposit Impactor
7 (MOUDI) measurements of inorganic particle components at three coastal urban sites in Tampa,
8 Florida during May 2002 using CMAQ's standard modal aerosol formulation (Kelly et al., 2010)
9 and a sectional formulation (Nolte et al., 2008). Kelly et al. (2011) evaluated size-composition
10 distributions of inorganic and carbonaceous PM against MOUDI data at five sites in California's
11 Central Valley as well as Bodega Bay and Sequoia during a wintertime episode. Also, Zhang et
12 al. (2006) evaluated CMAQ predictions of total particle volume distributions in Atlanta, and
13 Elleman et al. (2010) evaluated predictions of total particle mass in two sub-micron size ranges in
14 the Pacific Northwest. These studies indicate that CMAQ often overpredicts the peak diameter of
15 PM mass-size distributions and the widths of the lognormal particle modes. Kelly et al. (2011)
16 reported that in some urban areas (e.g., Fresno, California) CMAQ adequately predicted the
17 observed peak diameter for inorganic components but overpredicted the peak diameter of the
18 organic and elemental carbon distributions. Overpredictions of particle diameter were found to
19 lead to underpredictions of the PM mass in the sub-2.5 μm size range (PM_{2.5}).

20 The scarcity of impactor data has prevented any model evaluation of size-composition
21 distributions across a continental-scale domain. Such an evaluation would enhance our confidence
22 in models for assessing the human health and ecosystem effects of PM. From 2001–2005, a pair
23 of field campaigns was conducted on a large geographic scale to yield size-segregated impactor
24 measurements of the inorganic PM composition at 14 rural sites across the United States and
25 Canada (Zhang et al., 2008; Lee et al., 2008a). In this paper, we evaluate size-composition
26 distributions modeled by CMAQ against impactor measurements collected during these two
27 campaigns, as well as urban-scale campaigns conducted in Pittsburgh and Tampa. We identify the
28 regions and seasons where model performance is best as well as those where further model
29 development is needed. Some implications on future evaluations of CMAQ output against routine
30 measurements of PM_{2.5} composition are also discussed.

31

1 **2 Data**

2 **2.1 CMAQ simulations**

3 The measurements used in this study were taken during discrete sampling periods spread across
4 the years 2001–2005; therefore several years of CMAQ model simulations were required in order
5 to create a comprehensive analysis dataset. Four years of CMAQ simulations were conducted,
6 covering the period 2002–2005. The CMAQ model configuration was the same for all simulations,
7 with the only differences being in the year-specific emission and meteorological input data. The
8 simulations utilized CMAQ version 5.0.1, which includes updates to the treatment of
9 anthropogenic fugitive dust and windblown dust (Appel et al., 2013), as well as NH₃ bi-directional
10 surface exchange (Bash et al., 2013). The simulations were performed for a domain covering the
11 Continental United States (CONUS) and southern Canada utilizing 12-km by 12-km horizontal
12 grid spacing and 35 vertical layers, with the top of the lowest model layer at approximately 20 m.
13 Lateral boundary conditions (BCs) for the CMAQ simulations were obtained from monthly
14 median concentrations from a GEOS-Chem (Bey et al., 2001) model simulation of the year 2005
15 (the same BCs were used for all four years) using the procedure described by Henderson et al.
16 (2014). Other model options employed include the AERO6 aerosol module, the Carbon Bond
17 chemical mechanism that includes toluene and chlorine chemistry (CB05TUCL; Sarwar et al.
18 2011), and online computation of photolysis rates.

19 Meteorological data were provided from Weather Research and Forecast (WRFv3.3; Skamarock
20 et al., 2008) model version 3.3 simulations of 2002–2005. The WRF model simulations were
21 performed using 35 vertical layers extending up to 50 hPa, the Pleim-Xiu land-surface model (PX-
22 LSM; Pleim and Xiu, 1995), the ACM2 planetary boundary layer (PBL) scheme (Pleim, 2007ab),
23 the Kain-Fritsch cumulus parameterization scheme (Kain, 2004), the Morrison microphysics
24 scheme (Morrison et al., 2008) and four-dimensional data assimilation with no nudging in the PBL.
25 Version 4.0 of the Meteorology Chemistry Interface Processor (MCIPv4.0; Otte and Pleim, 2010)
26 was used to prepare WRF outputs for CMAQ using the same 35-layer vertical structure as in WRF.
27 Hourly, gridded emission data from non-mobile sources between 2002–2005 were created using
28 version 3.1 of the Sparse Matrix Operator Kernel Emissions (SMOKEv3.1; Houyoux et al., 2000)
29 and are based on the 2002 National Emissions Inventory (NEI) for the years 2002–2004 (2003 and

1 2004 are projected from 2002) and the 2005 NEI for 2005. Continuous emission monitoring
2 (CEM) data were used for the electric generating units sector. Wildfire emissions were based on
3 daily fire detections from the Hazard Mapping System and the Sonoma Technology SMARTFIRE
4 system (http://www.getbluesky.org/smartfire/docs/Raffuse_2007.pdf). Hourly mobile emissions
5 were created using year-specific traffic and meteorological data in version 2010b of the Motor
6 Vehicle Emission Simulator (MOVESv2010b; <http://www.epa.gov/otaq/models/moves>). PM_{2.5}
7 emissions of eight trace metals, including Mg²⁺, Ca²⁺, and K⁺, were speciated using the profiles in
8 Reff et al. (2009). Other model configuration options affecting emissions include online emissions
9 of accumulation and coarse mode Na⁺, Cl⁻, SO₄²⁻, Mg²⁺, Ca²⁺, and K⁺ from sea spray (Kelly et al.,
10 2010), online NO emissions using lightning flash counts from the National Lightning Detection
11 Network (NLDN; Allen et al., 2012); BELD3 land-use for gridded fractional crop distributions;
12 version 3.1.4 of the Biogenic Emissions Inventory System (BEIS v3.1.4; Vukovich and Pierce,
13 2002) for online biogenic emissions; the 2001 version of the National Land Characterization
14 Database (NLCD) for land-use data; and NH₃ emissions from fertilizer based on an Environmental
15 Policy Integrated Climate (EPIC; Cooter et al., 2012) simulation using 2002 fertilizer sales data.

16 **2.2 MOUDI measurements**

17 The MOUDI measurements used in this study are from four distinct datasets, with one dataset
18 consisting of observations from wilderness sites located in several Canadian provinces (Zhang et
19 al., 2008), another set consisting of sites primarily located in U.S. National Parks (Malm et al.,
20 2005; Lee et al., 2008a), a smaller dataset from sites available during the Bay Region Atmospheric
21 Chemistry (BRACE) study in Tampa, Florida (Evans et al., 2004), and finally a dataset collected
22 during the Pittsburgh Air Quality Study (Cabada et al., 2004). Data are available from 18 distinct
23 sites covering 24 observation periods generally ranging in length from two to four weeks and
24 covering each season of the year. To our knowledge, this collection represents the most
25 comprehensive dataset collected to date characterizing inorganic PM size-composition
26 distributions for multiple locations across the U.S. and Canada and under diverse meteorological
27 conditions. A brief description of the MOUDI data is provided below and a summary of the site
28 locations and observation dates is provided in Table 1, with locations illustrated in Figure 1.

29 Aerosol ion (SO₄²⁻, NO₃⁻, NH₄⁺, Cl⁻, Na⁺, Mg²⁺, Ca²⁺ and K⁺) size distributions were measured at
30 eight Canadian sites (i.e. ALG, BRL, CHA, EGB, FRS, KEJ, LED and SPR) (Zhang et al., 2008).

1 The number of samples and the sample duration varied among monitors, with 7 being the fewest
2 and 24 being the most samples taken during any one observation period, while the shortest sample
3 duration was 6 hours and the longest 152 hours. Standard ion chromatography was used for
4 analyses of all filters after extraction in deionized water. Additional details regarding these
5 measurements can be found in Zhang et al. (2008).

6 Size distributions of the same particle ions were collected at the BON, SGO, GRC, GSM, YOS
7 and BRG sites in the U.S. To ensure adequate mass collection at these rural locations, samples
8 were typically collected over a 48 h period, with the exception of Yosemite NP which used 24 h
9 sampling periods. A total of seven study periods are available from these sites in 2002–2004, with
10 one study period in 2002 from mid-July through mid-August (YOS), five study periods in 2003
11 occurring in February (BON), April (SGO1), May (GRC), July (SGO2) and November (BRG),
12 and one study period in 2004 from mid-July through mid-August (GSM). Additional details
13 regarding these data can be found in Lee et al. (2008a).

14 Aerosol ion size distributions in three urban locations were collected during the BRACE study in
15 Florida in 2002 at the AZP, GAN and SYD sites and in PIT in January 2002 (Table 1). Similar to
16 the other two datasets described above, the BRACE data were collected using MOUDI samplers
17 with 8 or 10 fractionation stages, an inlet height of 2 m, and a flow rate of 30 L min⁻¹ for sample
18 durations of approximately 23 h. Samples were collected on 15 days at the AZP and GAN sites
19 and 14 days at the SYD site between 4 May and 2 June for a total of 58 samples. Samples at the
20 Pittsburgh site were collected during January 1–17 for a total of 11 samples. Additional details
21 regarding the BRACE data can be found in Evans et al. (2004) and Nolte et al. (2008), while
22 additional details on the Pittsburgh data can be found in Cabada et al. (2004) and Stanier et al.
23 (2004).

24 **2.3 Data pairing and analysis**

25 The particle size distribution data consist of multiple measurements taken over a period of several
26 weeks. Since the analysis is focused on broad persistent features rather than day-to-day variability,
27 the data here are averaged into a single observed and modeled size distribution for each ion for
28 each campaign listed in Table 1, where the model output is averaged over the days and times
29 corresponding to each sampling period. The CMAQ aerosol model uses three lognormal modes

1 (Aitken, accumulation, and coarse) to represent particle size distributions (Binkowski and Roselle,
 2 2003), whereas the observations are separated into discrete size bins. To facilitate comparison
 3 between the model and the observations, the three modes in the model are summed to produce a
 4 single smooth curve. For each mode j , mass concentrations $M_j = \sum_i M_{ij}$ are obtained from the
 5 CMAQ hourly average concentration (ACONC) files, where M_{ij} is the mass of constituent i in
 6 mode j . Modal parameters $D_{g,j}$, $\sigma_{g,j}$, and $M_{3,j}$ are taken from the aerosol diagnostic (AERODIAM)
 7 files, where $D_{g,j}$ is the geometric number mean diameter of mode j , $\sigma_{g,j}$ is the geometric standard
 8 deviation of mode j , and $M_{3,j}$ is the third moment of mode j . Particle densities ρ_j are calculated as

$$9 \quad \rho_j = \frac{10^{-12} \cdot 6}{M_{3,j}} M_j.$$

10 The geometric volume mean diameters D_{gv} are calculated from the number mean diameters using
 11 the Hatch-Choate relation

$$12 \quad D_{gv,j} = D_{g,j} \sqrt{\rho_j} \exp(3 \ln^2 \sigma_{g,j})$$

13 where the multiplication by $\sqrt{\rho_j}$ puts the expression in terms of the particle aerodynamic diameter
 14 for consistency with the measurements. The size distribution at each hour t is then computed as

$$15 \quad \frac{dM}{d \ln D_p}(D_p, t) = \sum_{j=1}^3 \frac{M_j}{\sqrt{2\pi} \ln \sigma_{g,j}} \exp \frac{-(\ln D_p - \ln D_{gv,j})^2}{2 \ln^2 \sigma_{g,j}}$$

16 The above equation is discretized by $\ln D_p$, and the discretized values are computed for each hour
 17 before finally computing the temporally averaged size distribution.

18 In CMAQ v5.0, accumulation mode emissions from sea spray are chemically speciated into Na^+ ,
 19 Cl^- , SO_4^{2-} , Mg^{2+} , Ca^{2+} , and K^+ components, but coarse mode sea spray cations are lumped into a
 20 single species for computational efficiency. Concentrations of individual chemical components in
 21 the coarse mode are computed from the modeled sea spray cations (ASEACAT), soil dust
 22 (ASOIL), and coarse primary emissions (ACORS) using composite weighting factors based on
 23 profiles in the SPECIATE database (Simon et al., 2010).

24

25 **3 Evaluation of Size Distributions**

1 In this section CMAQ modeled size-composition distributions are compared to the MOUDI
2 measurements. For brevity, a few representative sites and time periods are presented for each ion.
3 Plots of the average modeled and measured size distributions for all 24 campaigns listed in Table
4 1 are available in the Supplementary Information for each of the inorganic ions analyzed.

5 **3.1 SO₄²⁻ and NH₄⁺**

6 Modeled and observed SO₄²⁻ size distributions at each site and averaged over each sampling
7 campaign are shown in Supplemental Figure S1. The model generally captures the variability in
8 the SO₄²⁻ size distribution across different sites and different seasons. As shown in Figure 2, the
9 model accurately reproduces the observed SO₄²⁻ size distribution at many sites, including LED2,
10 SPR2, SGO1, and SYD. However, the model fails to capture the accumulation mode peak
11 observed in many of the campaigns (e.g., ALG1 and GSM), and often the modeled peak diameter
12 is shifted to larger sizes (e.g., BRL and CHA2) than indicated by the measurements.

13 The model performance for particle NH₄⁺ (Figure 3 and Supplemental Figure S2) generally follows
14 that of SO₄²⁻, with the model tending to underestimate the accumulation mode peak concentration
15 and overestimating the aerodynamic diameter where the peak occurs. Modeled and observed NH₄⁺
16 size distributions are generally in good agreement at those sites where SO₄²⁻ performance is best
17 (i.e., LED2, SPR2, and SYD), though there is a large NH₄⁺ underprediction at SGO1 in contrast
18 to good SO₄²⁻ performance there. This behavior is consistent with recent studies that have reported
19 that NH₃ emissions in southern California's South Coast Air Basin are underestimated in the NEI
20 (Nowak et al., 2012; Kelly et al., 2014). Similarly to the performance for SO₄²⁻, the model largely
21 underestimates the NH₄⁺ accumulation mode peak and overestimates the diameter at which the
22 peak occurs at ALG1, GSM, BRL, and CHA2.

23 **3.2 Na⁺ and Cl⁻**

24 Sea spray is the principal source of Na⁺ and, at most locations, the dominant source of Cl⁻ as well.
25 Average modeled and observed Na⁺ size distributions are plotted for the coastal and near-coastal
26 sites in Figure 4. Cl⁻ size distributions generally follow those for Na⁺ and accordingly they are not
27 further discussed here, though Na⁺ and Cl⁻ plots across all the campaigns are presented in
28 Supplemental Figures S3 and S4. CMAQ generally captures the Na⁺ size distributions and
29 elevated concentrations at the coastal sites, i.e., the BRACE sites (AZP, GAN, and SYD), as well

1 as BRG and KEJ. At most of the other sites, Na⁺ concentrations are very low; often concentrations
2 at these sites are near the detection limit, and confidence in the measurements is relatively low
3 (Zhang et al. 2008). CMAQ correctly simulates that Na⁺ concentrations are low at these low-
4 concentration sites, though size distributions do not agree very well with measurements
5 (Supplemental Figure S3). The ALG site near Lake Superior is not impacted by sea spray; the
6 relatively high Na⁺ concentrations in ALG1 are due to the application of salt to roads to prevent
7 ice formation during the winter (Zhang et al. 2008). As this Canadian road salt is not in the U.S.
8 NEI, it is not surprising that the model is unable to capture this peak. SGO is about 100 km inland
9 from the Pacific Ocean. CMAQ's relatively poor performance for Na⁺ at SGO2 is likely
10 attributable to inaccuracies in sea spray emissions or to errors in transport to the SGO site.

11 The concentration of Cl⁻ in fresh sea spray aerosol is proportional to its abundance in seawater.
12 While Na⁺ and other sea salt cations are chemically inert, under certain conditions Cl⁻ in aged sea
13 spray particles can be displaced by condensed gas-phase acids, such as HNO₃. The percentage of
14 chloride depleted can be defined as (Yao and Zhang, 2012)

$$15 \quad \text{Cl}_{\text{depletion}}^{-}(\%) = \frac{\alpha[\text{Na}^{+}] - [\text{Cl}^{-}]}{\alpha[\text{Na}^{+}]} \times 100$$

16 where [Na⁺] and [Cl⁻] are molar equivalent concentrations and α is the ratio of the relative molar
17 abundance of Cl⁻ to Na⁺ in seawater, equal to 1.164 in CMAQ. The modeled percentages of
18 chloride depletion are compared to the individual measurements at near-coastal sites in Figure 5.
19 Consistent with previous results of Kelly et al. (2010), the model frequently underestimates the
20 moderate (25-50%) levels of chloride depletion seen at the BRACE sites (AZP, GAN, and SYD),
21 which are within 20 km or less from Tampa Bay. The negative bias in the amount of chloride
22 depletion is slightly greater at BRG (not shown). For the rural coastal KEJ site in Nova Scotia,
23 the model slightly underestimates the chloride depletion during the fall campaign (KEJ2), but
24 severely underestimates the frequently near-total depletion observed during the summer (KEJ1)
25 (Yao and Zhang, 2012). For the springtime campaign SGO1, the calculated Cl⁻ depletion is
26 overestimated, in part due to significant contributions of sodium from the primary species ASOIL
27 and ACORS. For the summer SGO2 campaign, the model correctly simulates chloride depletions
28 approaching 100%, while at YOS the modeled degree of chloride depletion is sometimes greater
29 than observed. Highly time-resolved measurements were made using a Particle-Into-Liquid

1 Sampler (PILS) at the same locations and times as the MOUDI measurements that are the focus
2 of this study (Lee et al., 2008b). The PILS measurements show that NO_3^- peaks coincide with Cl^-
3 dropping below detection limits at YOS and SGO2, providing strong evidence of chloride
4 displacement from condensation of HNO_3 . The PILS data further demonstrate that aerosol
5 concentrations varied substantially on much shorter timescales than could be captured by the
6 integrated MOUDI measurements, which partially accounts for the scatter in Figure 5.

7 **3.3 Mg^{2+} , Ca^{2+} and K^+**

8 At coastal sites, modeled Mg^{2+} concentrations generally follow modeled Na^+ concentrations in
9 accordance with their relative abundances in seawater, and model performance for Mg^{2+} generally
10 follows that for Na^+ at these sites. At AZP (Figure 6) as well as GAN, SYD, BRG, KEJ1, KEJ2,
11 ALG1, and SGO2 (Supplemental Figure S6), the observed and modeled Mg^{2+} size distributions
12 have the same relationship to each other as the corresponding Na^+ size distributions at those sites.
13 At BRL, GRC, and YOS, Mg^{2+} is likely to have a crustal rather than oceanic origin. At these
14 western sites, Mg^{2+} is underpredicted (Figure 6), consistent with findings of Appel et al. (2013).
15 Unlike the behavior for Mg^{2+} , modeled Ca^{2+} is notably underpredicted at coastal sites (Figure 6
16 and Supplemental Figure S7). This suggests that there is a source of Ca^{2+} at those sites not captured
17 by the model. On the other hand, modeled Ca^{2+} is higher than modeled Mg^{2+} at BRL, GRC, and
18 YOS, in better agreement with observations, indicating that the coarse mode Ca^{2+} at those sites is
19 due to contributions from anthropogenic fugitive dust or soils rather than sea spray. The chemical
20 speciation of windblown dust and directly emitted coarse PM is derived from four California desert
21 soil profiles in SPECIATE. Because these profiles did not report Mg, these sources do not
22 contribute to Mg^{2+} concentrations modeled by CMAQ. The relatively good model performance
23 for Ca^{2+} and underprediction of Mg^{2+} at these sites suggest that the Mg^{2+} speciation factors for
24 primary coarse PM and windblown dust should be revisited.

25 Model performance for K^+ is notably better than for Ca^{2+} , with the model reasonably capturing the
26 observed pattern at most sites (Figure 6 and Supplemental Figure S7). K^+ is known to be emitted
27 from biomass burning in addition to the sea spray and dust sources that also impact Ca^{2+} . The
28 impact of the combustion source of K^+ is evident in the smaller peak diameters for the K^+ and the
29 Mg^{2+} and Ca^{2+} observed distributions. The model simulates a bimodal distribution at GRC where
30 the observed distribution was a broad single mode, and the coarse mode is underpredicted at YOS.

1 Overall however, the model does well in simulating the observed K^+ particle distribution at the
2 majority of the Canadian and U.S. sites.

3 **3.4 NO_3^-**

4 Aerosol NO_3^- is formed almost entirely from condensation of gas-phase HNO_3 on existing
5 particles. Moreover, the degree of gas-particle mass transfer for nitrate is thermodynamically
6 driven, and is a strong function of inorganic particle composition as well as temperature and
7 relative humidity. As a result, the NO_3^- size distribution depends on the distribution of other ions,
8 especially SO_4^{2-} and NH_4^+ , making it particularly challenging to model accurately (Figure 7 and
9 Supplemental Figure S8). Model performance for NO_3^- is generally good at ALG1, CHA1, and
10 KEJ1, though the coarse mode is somewhat underpredicted at these sites, while the accumulation
11 mode is slightly overpredicted at LED2. Despite the greater surface area of the fine modes, NO_3^-
12 often resides in the coarse mode when the fine modes are too acidic from condensation of H_2SO_4 ,
13 which has lower vapor pressure than HNO_3 under ambient conditions. At BRL and BON, the
14 modeled size distribution is broader and shifted slightly to larger particles than measured by the
15 MOUDI. At SGO1 and YOS, particle NO_3^- is significantly underestimated. These errors in
16 modeled NO_3^- concentrations can be attributed to underestimated levels of accumulation-mode
17 NH_4^+ at SGO1 and underestimated coarse-mode Na^+ at YOS (cf. Figure 7 and Supplementary
18 Figure S3).

19 **3.5 Modeled $PM_{2.5}$**

20 In the U.S. as well as many other countries, air quality regulations for particulate matter are based
21 on the total mass of particles with aerodynamic diameters less than $2.5 \mu m$ ($PM_{2.5}$). Most CMAQ
22 model evaluations, however (e.g., Appel et al., 2008), have used the sum of PM in the Aitken (*i*)
23 and accumulation (*j*) modes (i.e. PM_{10}), to represent $PM_{2.5}$. As noted by Jiang et al. (2006), PM_{10}
24 and $PM_{2.5}$ are conceptually distinct quantities that sometimes differ significantly. Since the release
25 of CMAQ v4.5 in 2005, the capability has existed to output additional variables to a diagnostic file
26 to facilitate rigorous calculation of modeled $PM_{2.5}$, but PM_{10} is still typically used for model
27 evaluation (Foley et al., 2010). As a further evaluation of CMAQ modeled aerosol size
28 distributions, here we compare modeled $PM_{2.5}$ to the traditional PM_{10} calculations and to observed
29 total $PM_{2.5}$ from the IMPROVE, CSN and AQS networks for 2002.

1 The mass-weighted fractions of the accumulation mode and coarse mode in the PM_{2.5} size range
2 averaged over the summer and winter seasons are shown in Figure 8. Although during the winter
3 the vast majority of the accumulation mode is smaller than 2.5 μm, during the summer up to 10-
4 12% of the accumulation mode is greater than 2.5 μm in size. The fractional contribution of the
5 coarse mode to PM_{2.5} is fairly uniform, ranging from 10-15%, though there are a few areas where
6 the contribution exceeds 20%. Modeled PM_{2.5} is 0.3-1.2 μg m⁻³ lower than PM₁₀ across a large
7 portion of the eastern U.S. during the summer (Figure 9), primarily due to the greater contributions
8 of SO₄²⁻, NO₃⁻, NH₄⁺ and EC to PM₁₀ than PM_{2.5} concentrations. In the western U.S., PM_{2.5} values
9 are sporadically higher (primarily in Texas, New Mexico, Arizona and southern California) due
10 almost exclusively to the greater contributions of soil (i.e. Al, Si, Ca, Fe and Ti) to PM_{2.5} than PM₁₀
11 that result from the tail of the coarse mode overlapping the PM_{2.5} size range. The relative
12 differences are 4-12% in the eastern U.S. during summer and 4-20% in the western U.S.
13 (Supplementary Figure S9).

14 Histograms of the difference in CMAQ daily mean aerosol concentrations (modeled PM_{2.5} –
15 modeled PM₁₀) at IMPROVE, CSN and AQS-FRM sites for 2002 are also shown in Figure 9. The
16 distribution of mean differences is predominantly negative, particularly during summer and fall
17 (not shown), indicating that PM₁₀ is generally greater than PM_{2.5}. For all seasons, the differences
18 in PM_{2.5} and PM₁₀ typically fall between ±1 μg m⁻³.

19 The mean bias (MB), mean error (ME) and root mean square error (RMSE) as computed against
20 the IMPROVE, CSN and AQS-FRM observations using modeled PM_{2.5} and PM₁₀ values is
21 provided in Table 2. The difference in network- and seasonally-averaged MB, ME, and RMSE
22 computed using PM_{2.5} and PM₁₀ is generally small. For winter, spring, and fall, average PM_{2.5} is
23 0.04-0.20 μg m⁻³ less than PM₁₀. Since the model is generally positively biased with respect to
24 observations during those seasons, using PM_{2.5} rather than PM₁₀ results in slightly improved
25 performance statistics. The difference between PM_{2.5} and PM₁₀ is larger (more negative) during
26 the summer, and since the model is generally negatively biased then, the MB, ME, and RMSE are
27 all slightly worse for PM_{2.5} than for PM₁₀. The differences during the summer are still small,
28 however, averaging 0.30 μg m⁻³ for MB, 0.22 μg m⁻³ for ME, and 0.21 μg m⁻³ for RMSE. Overall,
29 the aggregated model performance using modeled PM_{2.5} and PM₁₀ is nearly the same, with the
30 average difference (PM_{2.5} – PM₁₀) in MB, ME and RMSE across all seasons of -0.15, 0.02 and
31 0.02 μg m⁻³, respectively. Therefore, while the difference between PM_{2.5} and PM₁₀ values for any

1 particular observation site and time may be important, the difference in model performance
2 between the two values is relatively small on average. The difference in the two methods for
3 estimating PM_{2.5} is likely to be even smaller when the models are applied in a relative sense for a
4 regulatory context (Baker and Foley, 2011).

5 In the version of CMAQ (v4.3) used by Jiang et al. (2006), there was very little mass in the coarse
6 mode, and this mode was modeled as being chemically inert. Thus, PM₁₀ was always greater than
7 PM_{2.5} in that version. Because the model was generally positively biased with respect to
8 measurements, using the size distribution to compute PM_{2.5} improved model performance
9 statistics. There have been several updates to the CMAQ aerosol model since the version used by
10 Jiang et al. (2006). For this discussion, the most significant of these are the reduction of
11 overestimated unspesiated PM_{2.5} (i.e., PMOTHER; Appel et al., 2008; Foley et al., 2010; Appel et
12 al., 2013), and the treatment of gas-particle nitrate mass transfer to and from coarse mode particles
13 (Kelly et al., 2010). As a result, the consequence of estimating PM_{2.5} concentrations by using the
14 modeled size distributions rather than by summing the masses in the Aitken and accumulation
15 modes has been changed such that it does not always improve model performance.

16 **4 Model Sensitivities**

17 Four additional simulations are conducted to assess the sensitivity of modeled size distributions to
18 changes in the aerosol model. The “BASE” model configuration used for the sensitivity runs
19 contains various updates from CMAQ v5.0.1, but overall results of the BASE simulation used for
20 these sensitivity studies are very similar to those presented in Section 3. The three sensitivity
21 studies include an adjustment to the apportionment of PM emissions between modes and the
22 implementation of a new gravitational settling scheme, two changes that are planned to be included
23 in CMAQ v5.1 (scheduled for release in fall 2015). In addition, a third simulation is performed
24 where the allowable particle mode widths (i.e. geometric standard deviations) in the model are
25 constrained to a relatively narrow range. The details of each sensitivity analysis are described in
26 the following three sub-sections. The sensitivity tests are each performed for May 2002 and
27 compared to data from the three BRACE sites in Tampa during that month.

28 **4.1 PM emissions adjustment**

1 Currently (i.e., in CMAQ v5.0.2), primary anthropogenic emissions of PM_{2.5} elemental carbon
2 (EC), organic carbon (OC), and non-carbonaceous organic matter (NCOM) are mostly (99.9%)
3 assigned to CMAQ's accumulation mode, with the remaining 0.1% assigned to the Aitken mode.
4 Primary anthropogenic emissions of other species (i.e., sulfate, nitrate, chloride, ammonium,
5 sodium, water, and "other") are 100% assigned to the accumulation mode. As noted by Elleman
6 and Covert (2010), these modal mass fractions are based on historical measurements that
7 underestimated ultrafine particles. In an effort to improve simulation of aerosol number size
8 distributions, Elleman and Covert (2010) updated particulate emissions size distributions based on
9 a review of modern measurements in regions dominated by urban, power-plant, and marine sources
10 at 4-15 km spatial scales. In the "PMEMIS" sensitivity test, the modal mass fractions for "urban"
11 PM emissions from Elleman and Covert (2010) (i.e., 10% Aitken mode, 90% accumulation mode)
12 were applied to all primary anthropogenic PM_{2.5} emissions. In addition, the modal parameters
13 characterizing the emitted particles (i.e., geometric mean volume diameter and standard deviation)
14 were modified. The updated emission parameters and their base case values are listed in Table 3.
15 Anthropogenic emissions of coarse PM, as well as sea spray and windblown dust, were unchanged.
16 The change in particle size distribution for SO₄²⁻ and Na⁺ at the three BRACE sites when
17 implementing the PM emissions adjustment is shown in Figure 10. Particle size distributions are
18 narrower and shifted toward smaller sizes in the PMEMIS simulation compared to the BASE
19 simulation, in better agreement with the observations. This model change affects only the fine
20 mode peak (e.g. SO₄²⁻) and does not impact the coarse mode peak (e.g. Na⁺). Overall, changing
21 the input PM emissions distribution improves CMAQ estimated particle size distribution
22 compared to the observations.

23 **4.2 Constrained mode widths**

24 CMAQ uses three lognormal modes to model the aerosol size distribution, where each mode is
25 characterized by three parameters: particle number, geometric mean diameter, and geometric
26 standard deviation (Binkowski and Roselle, 2003). Though the mode standard deviations (widths)
27 are calculated as prognostic variables within the aerosol code, they are constrained between the
28 values 1.05 and 2.50. Furthermore, due to numerical instabilities the coarse mode width is not
29 allowed to vary during condensation and evaporation (Kelly et al., 2010). CMAQ mode widths
30 often reach the allowed upper bound, which reduces confidence that they are being simulated

1 accurately. Several other state-of-the-science modal aerosol models use fixed mode widths (e.g.,
2 COSMO-ART (Vogel et al., 2009); MESSy/MADE3 (Kaiser et al., 2014)), though other models
3 also allow mode widths to vary (e.g., RAQM2/MADMS (Kajino et al., 2012)). To explore how
4 using fixed mode widths might affect CMAQ simulated size distributions, a model sensitivity
5 study “CONSIG” based on the PMEMIS simulation was conducted in which the modal standard
6 deviation constraints were modified from 1.05-2.50 to ± 0.1 from their emitted values, i.e., the
7 Aitken mode and accumulation mode standard deviations were constrained between 1.6 and 1.8,
8 while the coarse mode standard deviation was constrained between 2.1 and 2.3.

9 The difference in particle size distribution between the PMEMIS simulation and the CONSIG
10 simulation is also shown in Figure 10. Similar to the PMEMIS sensitivity, constraining the mode
11 widths tends to produce an accumulation mode peak that is narrower and shifted to smaller sizes
12 than the PMEMIS simulation, resulting in a better comparison against the observations. For the
13 coarse mode however, constraining the mode widths results in a wider and lower peak than the
14 PMEMIS simulations, which does not compare as well to the observations. Of course, the impact
15 on model performance is directly dependent on the values chosen to constrain the particle mode
16 widths, and alternative constraints could potentially improve performance for the coarse mode.
17 These results do suggest, however, that the modeled size distribution is sensitive to the treatment
18 of the mode widths, and that improvements in the algorithm that computes them would be
19 beneficial.

20 **4.3 Gravitational settling**

21 Although the CMAQ aerosol module simulates gravitational settling for particles in the lowest
22 model layer in computing their dry deposition velocities (Binkowski and Roselle, 2003), a
23 potential limitation of the approach is the absence of gravitational settling for particles above layer
24 1. As a result, coarse particles emitted or convectively mixed above the first model layer can
25 artificially remain aloft and be transported downwind farther than is realistic. As part of the
26 development for the fall 2015 release of the CMAQ model, a gravitational settling scheme has
27 been implemented in which settling velocities are calculated for accumulation and coarse mode
28 aerosol zeroth, second, and third moments in each grid cell. The method is a Stokes law approach
29 using the same equations used in computing aerosol deposition velocities to the surface in layer 1
30 [see equations A31-A32 in Binkowski and Shankar (1995)]. The settling velocities are then used

1 in a sedimentation sub-module to calculate the moment fluxes through model layers using a first-
2 order upstream relation.

3 The difference in average Na^+ size distributions simulated with and without gravitational settling
4 is shown in Figure 11. Because the impact of gravitational settling is significant only for larger
5 particles, there is no discernible effect on the fine-mode range of the aerosol size distribution when
6 gravitational settling is included. However, there is a slight shift in the coarse-mode size range,
7 with a higher peak concentration occurring at a smaller particle diameter. This peak tends to be
8 higher in the GRAV simulation due to particles settling from upper model layers into the lowest
9 model layer, increasing the overall surface layer concentration. Including the effects of
10 gravitational settling has only a very minor impact on modeled $\text{PM}_{2.5}$ mass.

11

12 **5 Summary**

13 Size resolved particle ion SO_4^{2-} , NO_3^- , NH_4^+ , Cl^- , Na^+ , Mg^{2+} , Ca^{2+} and K^+ measurements for sites
14 located throughout the United States and Canada in 2002-2005 were compared to CMAQv5.0.1
15 model output to assess the ability of the model to reproduce the observed particle mass size
16 distribution. A total of 24 different measurement campaigns (some sites measured in two different
17 seasons) were available across the four years. The model was generally able to reproduce the
18 observed SO_4^{2-} and NH_4^+ distributions at most of the sites, but tended to overestimate the peak
19 diameter and underestimate the peak particle concentration. NH_4^+ was substantially
20 underestimated at the SGO site, likely due to underestimated NH_3 emissions in California's South
21 Coast Air Basin.

22 CMAQ was generally able to capture the size distribution and higher concentrations of Na^+ and
23 Cl^- at coastal and near-coastal sites. The model also reasonably captures Mg^{2+} concentrations and
24 size distributions for those sites where Mg^{2+} originates from sea spray (e.g., the three BRACE sites
25 in Florida), but underpredicts at sites influenced by soil dust, particularly in the western portion of
26 the modeling domain. By contrast, the model substantially underpredicts Ca^{2+} at many coastal
27 sites while having better performance than for Mg^{2+} at some inland sites, which may be attributable
28 to errors in speciation profiles for various source categories, including windblown and
29 anthropogenic fugitive dust. K^+ , which has contributions from residential wood combustion and
30 wildfires as well as sea spray, exhibits somewhat better model performance than Ca^{2+} . Model

1 performance for NO_3^- was mixed, with good performance at some sites (e.g., BRL, CHA1, KEJ1,
2 and LED2), overpredicted concentrations in the accumulation mode size range at some sites (e.g.,
3 BRG, FRS, and SPR2), and substantially underestimated accumulation mode NO_3^- at SGO1 and
4 underestimated coarse particle concentrations at other sites (e.g., GRC, GSM, and YOS).

5 An examination of the difference in model performance between calculating $\text{PM}_{2.5}$ mass from the
6 modeled size distribution or by summing the masses in the Aitken and accumulation modes (PM_{11})
7 showed that using the size distribution parameters results in values which on average are smaller
8 by 0.3-1.2 $\mu\text{g m}^{-3}$. On a daily basis, the difference in total PM between the two methods was
9 usually less than 1 $\mu\text{g m}^{-3}$, regardless of season or year (the largest differences between the two
10 methods were observed in the summer). The difference in model performance between the two
11 methods in comparison to observations was also generally small, particularly when aggregated
12 across sites, and would likely be even smaller when the model is used in a relative sense (e.g. for
13 State Implementation Plan development).

14 It is important to note that this evaluation of the CMAQ modeled aerosol size distributions has
15 focused on the mass size distribution and has considered only inorganic species. As understanding
16 of the health impacts associated with particular PM components and size ranges develops (e.g.,
17 Delfino et al., 2011), evaluating carbonaceous and ultrafine particle size distributions in urban
18 environments could be valuable to support health and exposure applications. Similarly, as the state
19 of the science evolves toward more frequent use of the two-way coupled WRF-CMAQ model
20 (Wong et al., 2012) to capture the influence of air pollution on atmospheric dynamics, particularly
21 the effect on clouds (Yu et al., 2014) it will be important to evaluate modeled aerosol number and
22 surface area distributions as well.

23

24 **Code Availability**

25 CMAQ model documentation and released versions of the source code are available at [www.cmaq-](http://www.cmaq-model.org)
26 [model.org](http://www.cmaq-model.org). The updates described here, as well as model postprocessing scripts, are available upon
27 request.

28 **Acknowledgements**

1 We thank Taehyoung Lee (Colorado State University), Noreen Poor (University of South Florida),
2 and Charles Stanier (University of Iowa) for providing MOUDI measurements that helped make
3 this analysis possible. Brett Gantt and Rohit Mathur (U.S. EPA) provided constructive comments
4 in reviewing this manuscript. We thank Heather Simon and George Pouliot (U.S. EPA) for their
5 assistance with PM profiles in the SPECIATE database. The United States Environmental
6 Protection Agency through its Office of Research and Development supported the research
7 described here. It has been subjected to Agency review and approved for publication. The views
8 and interpretations in this publication are those of the authors and are not necessarily attributable
9 to their organizations.

10

11 **References**

12 Allen, D.J., Pickering, K.E., Pinder, R.W., Henderson, B.H., Appel, K.W., and Prados, A.:

13 Impact of lightning-NO on eastern United States photochemistry during the summer of 2006 as
14 determined using the CMAQ model, *Atmos. Chem. Phys.*, 12, 1737-1758, 2012.

15 Appel, K.W., Bhave, P.V., Gilliland, A.B., Sarwar, G., Roselle, S. J.: Evaluation of the
16 Community Multiscale Air Quality (CMAQ) model version 4.5: Sensitivities impacting model
17 performance; Part II - particulate matter, *Atmos. Environ.*, doi:10.1016/j.atmosenv.2008.03.036,
18 2008.

19 Appel, K. W., Pouliot, G. A., Simon, H., Sarwar, G., Pye, H. O. T., Napelenok, S. L., Akhtar, F.,
20 and Roselle, S. J.: Evaluation of dust and trace metal estimates from the Community Multiscale
21 Air Quality (CMAQ) model version 5.0, *Geosci. Model Dev.*, 6, 883-899, doi:10.5194/gmd-6-
22 883-2013, 2013.

23 Asgharian, B., Hofmann, W., and Bergmann, R.: Particle deposition in a multiple-path model of
24 the human lung, *Aerosol Sci. Technol.* 34(4), 332–339, 2001.

25 Baker, K. R. and Foley, K. M.: A nonlinear regression model estimating single source
26 concentrations of primary and secondarily formed PM_{2.5}, *Atmos. Environ.* 45, 3758-3767, doi:
27 10.1016/j.atmosenv.2011.03.074, 2011.

1 Bash, J. O., Cooter, E. J., Dennis, R. L., Walker, J. T., and Pleim, J. E.: Evaluation of a regional
2 air-quality model with bidirectional NH₃ exchange coupled to an agroecosystem model,
3 *Biogeosciences*, 10, 1635-1645, doi:10.5194/bg-10-1635-2013, 2013.

4 Bey, I., Jacob, D. J., Yantosca, R. M., Logan, J. A., Field, B. D., Fiore, A. M., Li, Q., Liu, H. Y.,
5 Mickley, L. J., and Schultz, M. G.: Global modeling of tropospheric chemistry with assimilated
6 meteorology: Model description and evaluation, *J. Geophys. Res.*, 106, 23073-23096, 2001.

7 Binkowski, F. S. and Roselle, S. J.: Models-3 Community Multiscale Air Quality (CMAQ)
8 model aerosol component: 1. Model description, *J. Geophys. Res.* 108, D6, 4183,
9 doi:10.1029/2001JD001409, 2003.

10 Binkowski, F. S. and Shankar, U.: The Regional Particulate Matter Model: 1. Model description
11 and preliminary results, *J. Geophys. Res.*, 100, D12, 26,191-26,209, 1995.

12 Cabada, J.C., Rees, S., Takahama, S., Khlystov, A., Pandis, S.N., Davidson, C.I., and Robinson,
13 A.L.: Mass size distributions and size resolved chemical composition of fine particulate matter at
14 the Pittsburgh supersite, *Atmos. Environ.*, 38(20), doi:10.1016/j.atmosenv.2004.03.004, 3127-
15 2141, 2004.

16 Cooter, E.J., Bash, J.O., Benson, V., and Ran, L.: Linking agricultural crop management and air
17 quality models for regional to national-scale nitrogen assessments, *Biogeosciences* 9, 4023-4035,
18 doi:10.5194/bg-9-4023-2012, 2012.

19 Delfino, R. J., Staimer, N., and Vaziri, N. D.: Air pollution and circulating biomarkers of
20 oxidative stress, *Air Qual. Atmos. Health*, 4, 37-52, 2011.

21 Elleman, R. A., and Covert, D. S.: Aerosol size distribution modeling with the Community
22 Multiscale Air Quality Modeling system in the Pacific Northwest: 3. Size distribution of particles
23 emitted into a mesoscale model, *J. Geophys. Res.*, 115, D3(16), doi:10.1029/2009JD012401,
24 2010.

25 Evans, M.C., Campbell, S.W., Bhethanabotla, V., and Poor, N.D.: Effect of sea salt and calcium
26 carbonate interactions with nitric acid on the direct dry deposition of nitrogen on Tampa Bay,
27 Florida, *Atmos. Environ.*, 38, doi:10.1016/j.atmosenv.2004.05.046, 4847-4858, 2004.

28 Foley, K.M., Roselle, S.J., Appel, K.W., Bhave, P.V., Pleim, J.E., Otte, T.L., Mathur, R., Sarwar,
29 G., Young, J.O., Gilliam, R.C., Nolte, C.G., Kelly, J.T., Gilliland, A.B., and Bash, J.O.:

1 Incremental testing of the Community Multiscale Air Quality (CMAQ) modeling system version
2 4.7, *Geosci. Model Dev.*, 3, 205-226, 2010.

3 Henderson, B. H., Akhtar, F., Pye, H. O. T., Napelenok, S. L., and Hutzell, W. T.: A database
4 and tool for boundary conditions for regional air quality modeling: description and evaluation,
5 *Geosci. Model Dev.*, 7, 339-360, 2014.

6 Houyoux, M. R., Vukovich, J. M., Coats Jr., C. J., Wheeler, N. J. M., and Kasibhatla, P.:
7 Emission inventory development and processing for the seasonal model for regional air quality,
8 *J. Geophys. Res.*, 105 (D7), 9079 – 9090, 2000.

9 Jiang, W.M., Smyth, S., Giroux, E., Roth, H., and Yin, D.Z.: Differences between CMAQ fine
10 mode particle and PM_{2.5} concentrations and their impact on model performance evaluation in the
11 lower Fraser Valley, *Atmos. Environ.*, 40 (26), 4973-4985, doi:10.1016/j.atmosenv.2005.10.069,
12 2006.

13 John, W., Wall, S.M., Ondo, J.L., and Winklmayr, W.: Modes in the size distributions of
14 atmospheric inorganic aerosol, *Atmos. Environ.*, 24 (9), 2349-2359, doi:10.1016/0960-
15 1686(90)90327-J, 1990.

16 Kain, J.S.: The Kain-Fritsch convective parameterization: an update, *J. Appl. Meteor.*, 43, 170-
17 181, 2004.

18 Kaiser, J.C., Hendricks, J., Righi, M., Riemer, N., Zaveri, R.A., Metzger, S., and Aquila, V.: The
19 MESSy aerosol submodel MADE3 (v2.0b): description and a box model test, *Geosci. Model*
20 *Dev.*, 7, 1137-1157, 2014.

21 Kajino, M., Inomata, Y., Sato, K., Ueda, H., Han, Z., An, J., Katata, G., Deushi, M., Maki, T.,
22 Oshima, N., Kurokawa, J., Ohara, T., Takami, A., and Hatakeyama, S.: Development of the
23 RAQM2 aerosol chemical transport model and predictions of the Northeast Asian aerosol mass,
24 size, chemistry, and mixing type, *Atmos. Chem. Phys.*, 12, 11833-11856, 2012.

25 Kelly, J.T., Baker, K.R., Nowak, J.B., Murphy, J.G., Markovic, M.Z., VandenBoer, T.C, Ellis,
26 R.A., Neuman, J.A., Weber, R.J., Roberts, J.M., Veres, P.R., de Gouw, J.A., Beaver, M.R.,
27 Newman, S., and Misenis, C.: Fine-scale simulation of ammonium and nitrate over the South
28 Coast Air Basin and San Joaquin Valley of California during CalNex-2010, *J. Geophys. Res.*
29 *Atmos.*, 119, doi:10.1002/2013JD021290, 2014.

1 Kelly, J. T., Bhave, P. V., Nolte, C. G., Shankar, U., and Foley, K. M.: Simulating emission and
2 chemical evolution of coarse sea-salt particles in the Community Multiscale Air Quality
3 (CMAQ) model, *Geosci. Model Dev.*, 3, 257–273, 2010.

4 Kelly, J. T., Avise, J., Cai, C., and Kaduwela, A. P.: Simulating particle size distributions over
5 California and impact on lung deposition fraction, *Aerosol Sci. Technol.*, 45(2), 148-162,
6 doi:10.1080/02786826.2010.528078, 2011.

7 Lee, T., Yu, X.-Y., Ayres, B., Kreidenweis, S.M., Malm, W.C., Collett Jr., J.L.: Observations of
8 fine and coarse particle nitrate at several rural locations in the United States, *Atmos. Environ.*,
9 42, 2720-2732, doi:10.1016/j.atmosenv.2007.05.016, 2008a.

10 Lee, T., Yu, X.-Y., Kreidenweis, S. M., Malm, W. C., Collett, J. L.: Semi-continuous
11 measurement of PM_{2.5} ionic composition at several rural locations in the United States, *Atmos.*
12 *Environ.*, 42, 6655-6669, doi:10.1016/j.atmosenv.2008.04.023, 2008b.

13 Marple, V.A., Rubow, K.L., Behm, S.M.: A microorifice uniform deposit impactor (MOUDI) –
14 description, calibration, and use, *Aerosol Sci. Technol.*, 14 (4), 434-446,
15 doi:10.1080/02786829108959504, 1991.

16 Morrison, H., Thompson, G., and Tatarskii, V.: Impact of cloud microphysics on the
17 development of trailing stratiform precipitation in a simulated squall line: comparison of one-
18 and two-moment schemes, *Mon. Wea. Rev.*, 137, 991-1007, 2009.

19 Nolte, C.G., Bhave, P.V., Arnold, J.R., Dennis, R.L., Zhang, K.M., and Wexler, A.S.: Modeling
20 urban and regional aerosols – Application of the CMAQ-UCD aerosol model to Tampa, a coastal
21 urban site, *Atmos. Environ.*, 42, 3179-3191, doi:10.1016/j.atmosenv.2007/12/059, 2008. Nowak,
22 J. B., Neuman, J.A., Bahreini, R., Middlebrook, A.M., Holloway, J.S., McKeen, S.A., Parrish,
23 D.D., Ryerson, T.B., and Trainer, M.: Ammonia sources in the California South Coast Air Basin
24 and their impact on ammonium nitrate formation, *Geophys. Res. Lett.*, 39, L07804,
25 doi:10.1029/2012GL051197, 2012.

26 Otte, T. L., and Pleim, J. E.: The Meteorology-Chemistry Interface Processor (MCIP) for the
27 CMAQ modeling system: updates through MCIPv3.4.1, *Geosci. Mod. Dev.*, 3, 243-256, 2010.

28 Pleim, J. E.: A combined local and non-local closure model for the atmospheric boundary
29 layer. Part 1: Model description and testing, *J. Appl. Meteor. Clim.*, 46, 1383-1395, 2007a.

1 Pleim, J. E.: A combined local and non-local closure model for the atmospheric boundary
2 layer. Part 2: Application and evaluation in a mesoscale model, *J. Appl. Meteor. Clim.*, 46,
3 1396-1409, 2007b.

4 Pleim, J. E., and Xiu, A.: Development and testing of a surface flux and planetary boundary layer
5 model for application in mesoscale models, *J. Appl. Meteor.*, 34, 16–32, 1995.

6 Reff, A., Bhave, P.V., Simon, H., Pace, T.G., Pouliot, G.A., Mobley, J.D., Houyoux, M.:
7 Emissions inventory of PM_{2.5} trace elements across the United States, *Environ. Sci. Technol.*, 43,
8 5790-5796, 2009.

9 Sarwar, G., Appel, K.W., Carlton, A.G., Mathur, R., Schere, K., Zhang, R., and Majeed, M.A.:
10 Impact of a new condensed toluene mechanism on air quality model predictions in the US,
11 *Geosci. Model Dev.*, 4, 183-193, doi:10.5194/gmd-4-183-2011, 2011.

12 Scheffe, R.S., Lynch, J.A., Reff, A., Kelly, J.T., Hubbell, B., Greaver, T.L., and Smith, J.T.: The
13 Aquatic Acidification Index: a new regulatory metric linking atmospheric and biogeochemical
14 models to assess potential aquatic ecosystem recovery, *Water Air Soil Pollut.*, 225:1838, 2014.

15 Simon, H., Baker, K.R., and Phillips, S.: Compilation and interpretation of photochemical model
16 performance statistics published between 2006 and 2012, *Atmos. Environ.*, 61, 124-139,
17 doi:10.1016/j.atmosenv.2012.07.012, 2012.

18 Simon, H., Beck, L., Bhave, P. V., Divita, F., Hsu, Y., Luecken, D., Mobley, J. D., Pouliot, G.
19 A., Reff, A., Sarwar, G., and Strum, M.: The development and uses of EPA’s SPECIATE
20 database, *Atmos. Pollut. Res.*, 1, 196-206, doi: 10.5094/APR.2010.026, 2010.

21 Skamarock, W. C., Klemp, J. B., Dudhia, J., Gill, D. O., Barker, D. M., Duda, M. G., Huang, X-
22 Y, Wang, W., and Powers, J. G.: A description of the advanced research WRF version 3. NCAR
23 Tech Note NCAR/TN 475 STR, 125 pp, [Available from UCAR Communications, P.O. Box
24 3000, Boulder, CO 80307.], 2008.

25 Stanier, C.O., Khlystov, A.Y., and Pandis, S.N.: Ambient aerosol size distributions and number
26 concentrations measured during the Pittsburgh Air Quality Study (PAQS). *Atmos. Environ.*,
27 38(20), 3275-3284, doi:10.1016/j.atmosenv.2004.03.020, 2004.

28 Stanier, C.O., Khlystov, A.Y., and Pandis, S.N.: Nucleation events during the Pittsburgh Air
29 Quality Study: Description and relation to key meteorological, gas phase, and aerosol parameters

1 special issue of aerosol science and technology on the findings from the fine particulate matter
2 supersite program, *Aerosol Sci. Tech.*, 38:S1, 253-264, 2010.

3 Vogel, B., Vogel, H. Bäumer, D., Bangert, M., Lundgren, K., Rinke, R., and Stanelle, T.: The
4 comprehensive model system COSTMO-ART—Radiative impact of aerosol on the state of the
5 atmosphere on the regional scale, *Atmos. Chem. Phys.* 9, 8661-8680, 2009.

6 Vukovich, J. and Pierce, T.: The Implementation of BEIS3 within the SMOKE Modeling
7 Framework, In Proceedings of the 11th International Emissions Inventory Conference, Atlanta,
8 Georgia, April 15-18, 2002. (Available online:
9 www.epa.gov/ttn/chief/conference/ei11/modeling/vukovich.pdf)

10 Wong, D. C., Pleim, J., Mathur, R., Binkowski, F., Otte, T., Gilliam, R., Pouliot, G., Xiu, A.,
11 Young, J. O., and Kang, D.: WRF-CMAQ two-way coupled system with aerosol feedback:
12 software development and preliminary results, *Geosci. Model Dev.*, 5, 299-312, 2012.

13 Xiu, A., and Pleim, J. E.: Development of a land-surface model. Part I: application in a
14 mesoscale meteorological model, *J. Appl. Meteor.*, 40, 192-209, 2001.

15 Yao, X. and Zhang, L.: Chemical processes in sea-salt chloride depletion observed at a Canadian
16 rural coastal site, *Atmos. Environ.* 46, 189-194, 2012.

17 Yu, S., Mathur, R., Pleim, J., Wong, D., Gilliam, R., Alapaty, K., Zhao, C., Liu, X.: Aerosol
18 indirect effect on the grid-scale clouds in the two-way coupled WRF-CMAQ: model description,
19 development, evaluation and regional analysis, *Atmos. Chem. Phys.*, 14, 11247-11285, 2014.

20 Zhang, Y., Liu, P., Pun, B., and Seigneur, C.: A comprehensive performance evaluation of
21 MM5-CMAQ for the summer 1999 Southern Oxidants Study episode—Part III: Diagnostic and
22 mechanistic evaluations, *Atmos. Environ.*, 40(26), 4856–4873, 2006.

23 Zhang, L., Vet, R., Wiebe, A., Mihele, C., Sukloff, B., Chan, E., Moran, M.D., and Iqbal, S.:
24 Characterization of the size-segregated water-soluble inorganic ions at eight Canadian rural sites,
25 *Atmos. Chem. Phys.*, 8, 7133-7151, 2008.

26

Table 1. Summary of the MOUDI data used in this study.

Code	Location	Comment	Latitude	Longitude	Dates	Reference
ALG1	Algoma, Ontario, Canada	influenced by road salt	47.04	-84.38	8-27 Feb 2003	Zhang et al. (2008)
ALG2					5-26 Jun 2003	
AZP	Azalea Park, Florida, U.S.	urban coastal	27.78	-82.74	4 May – 2 Jun 2002	Evans et al. (2004)
BON	Bondville, Illinois, U.S.	agricultural	40.05	-88.37	1 – 27 Feb 2003	Lee et al. (2008)
BRL	Bratt's Lake, Saskatchewan, Canada		50.20	-104.20	11 Feb – 4 Mar 2005	Zhang et al. (2008)
BRG	Brigantine National Wildlife Refuge, New Jersey, U.S.	coastal	39.46	-74.45	4 – 30 Nov 2003	Lee et al. (2008)
CHA1	Chalk River, Ontario, Canada		46.06	-77.40	22 Jan – 21 Feb 2004	Zhang et al. (2008)
CHA2					4 – 26 Jun 2004	
EGB	Egbert, Ontario, Canada		44.23	-79.78	6 – 13 Mar 2002	Zhang et al. (2008)
FRS	Frelighsberg, Quebec, Canada		45.05	-73.06	4 – 16 May 2002	Zhang et al. (2008)
GAN	Gandy Bridge, Florida, U.S.	urban coastal	27.97	-82.23	4 May – 2 Jun 2002	Evans et al. (2004)

GRC	Grand Canyon National Park, Arizona, U.S.	remote	35.97	-111.98	1 – 30 May 2003	Lee et al. (2008)
GSM	Great Smokies National Park, Tennessee, U.S.	remote	35.63	-83.94	22 Jul – 19 Aug 2004	Lee et al. (2008)
KEJ1	Kejimikujik, Nova Scotia, Canada	rural coastal	44.43	-65.21	29 Jun – 15 Jul 2002	Zhang et al. (2008)
KEJ2					25 Oct – 15 Nov 2003	
LED1	Lac Edouard, Quebec, Canada		47.68	-72.44	11 – 27 Aug 2003	Zhang et al. (2008)
LED2					17 Oct – 3 Nov 2003	
PIT	Pittsburgh, Pennsylvania, U.S.	Pittsburgh Supersite	40.44	-79.94	1 – 17 Jan 2002	Stanier et al. (2004)
SGO1	San Geronio Wilderness Area, California, U.S.	mountainous	34.19	-116.90	4 – 26 May 2003	Lee et al. (2008)
SGO2					1 – 30 Jul 2003	
SPR1	Sprucedale, Ontario, Canada		45.42	-79.49	17 Aug – 18 Sep 2004	Zhang et al. (2008)
SPR2					16 Nov – 12 Dec 2004	
SYD	Sydney, Florida, U.S.	urban coastal	27.97	-82.23	4 May – 2 Jun 2002	Evans et al. (2004)
YOS	Yosemite National Park, California, U.S.	mountainous	37.75	-119.59	15 Jul – 2 Sep 2004	Lee et al. (2008)

Table 2. Comparison of CMAQ PM model performance relative to observations at IMPROVE, CSN and AQS network sites during 2002 using the sum of masses in the Aitken and accumulation modes ($PM_{1\mu}$) and calculated using the modeled size distribution ($PM_{2.5}$).

Season	MB ($\mu\text{g m}^{-3}$)			ME ($\mu\text{g m}^{-3}$)			RMSE ($\mu\text{g m}^{-3}$)		
	$PM_{2.5}$	$PM_{1\mu}$	$PM_{2.5} - PM_{1\mu}$	$PM_{2.5}$	$PM_{1\mu}$	$PM_{2.5} - PM_{1\mu}$	$PM_{2.5}$	$PM_{1\mu}$	$PM_{2.5} - PM_{1\mu}$
Winter (DJF)	2.38	2.42	-0.04	5.19	5.28	-0.09	8.68	8.73	-0.05
Spring (MAM)	0.46	0.53	-0.07	3.64	3.65	-0.01	6.07	6.11	-0.04
Summer (JJA)	-3.60	-3.30	-0.30	5.85	5.63	0.22	9.90	9.69	0.21
Fall (SON)	0.96	1.16	-0.20	4.77	4.79	-0.02	7.98	8.01	-0.03
Average	0.05	0.20	-0.15	4.86	4.84	0.02	8.16	8.14	0.02

Table 3. Parameters for Aitken and accumulation mode particulate emissions for the BASE run and PMEMIS sensitivity case.

mode	Species	BASE			PMEMIS sensitivity		
		Mass Fraction	D_{gv} (μm)	σ_g	Mass fraction	D_{gv} (μm)	σ_g
Aitken	EC/OC/NCOM	0.001	0.030	1.7	0.10	0.060	1.7
	Other	0.000					
accumulation	EC/OC/NCOM	0.999	0.300	2.0	0.90	0.280	1.7
	Other	1.000					

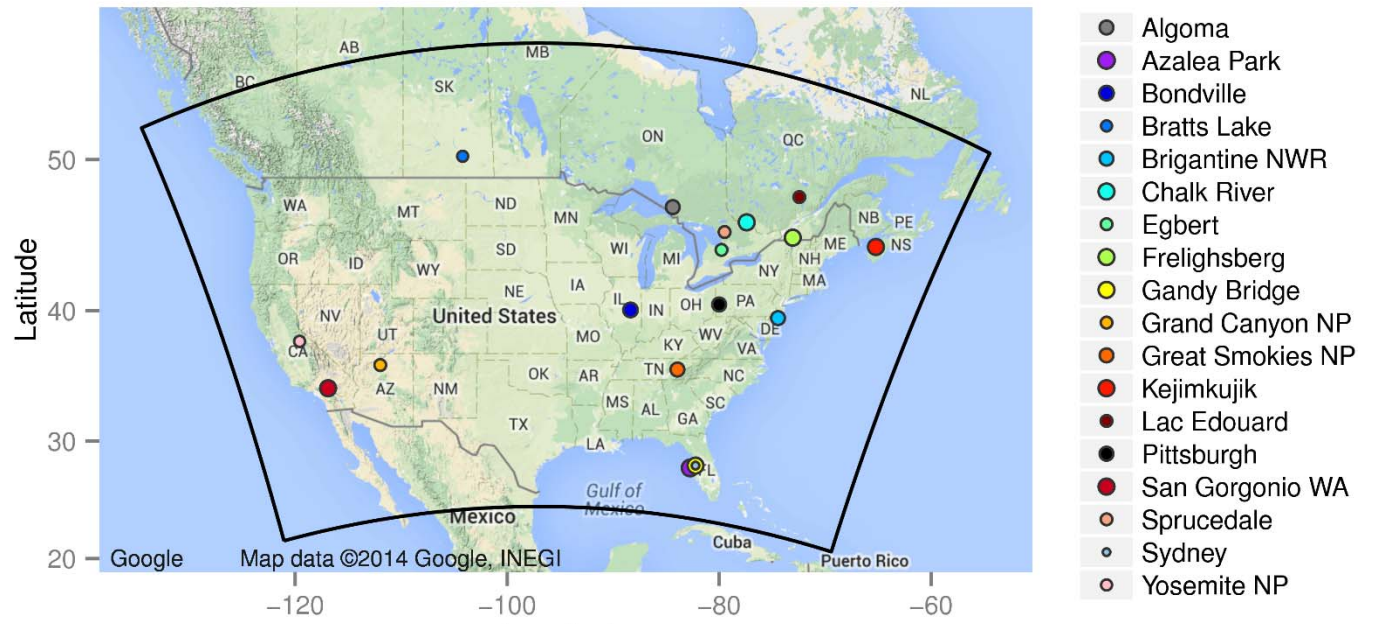


Figure 1. Location of the MOUDI sites used in this study.

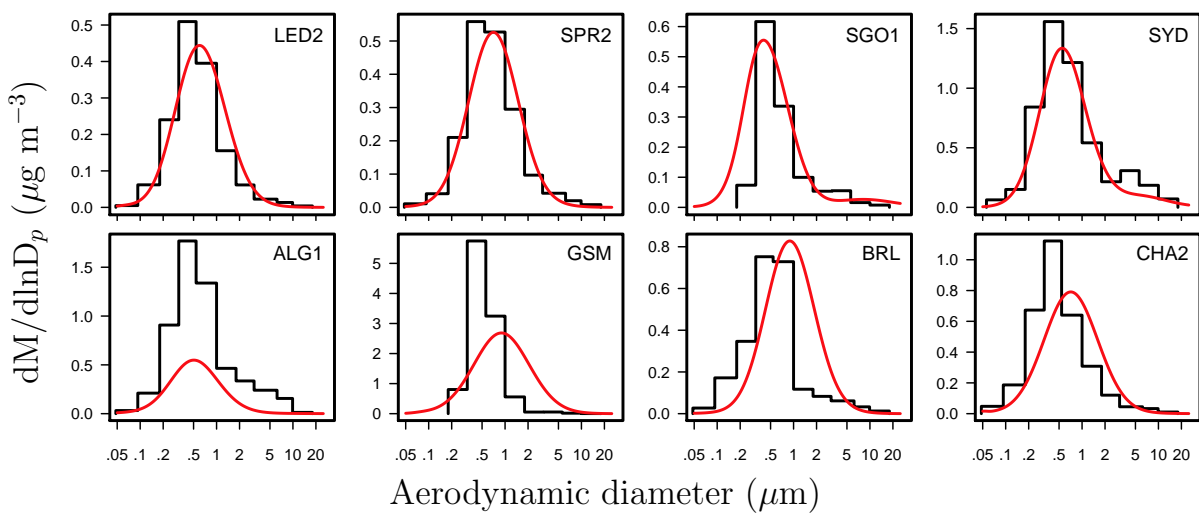


Figure 2: Average observed (black) and modeled (red) SO_4^{2-} size distributions at representative sites.

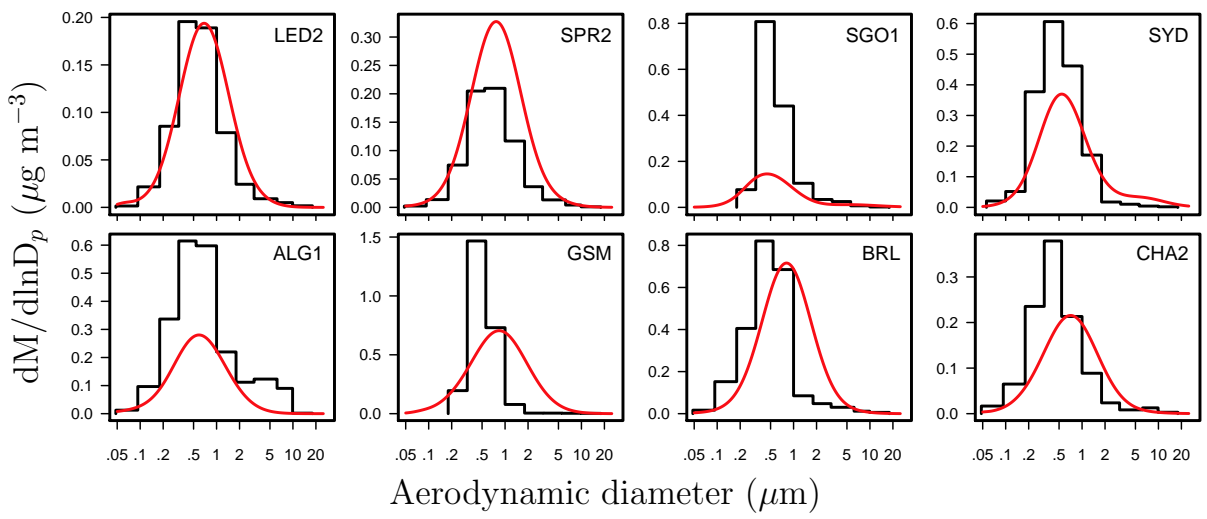


Figure 3: Average observed (black) and modeled (red) NH_4^+ size distributions at representative sites.

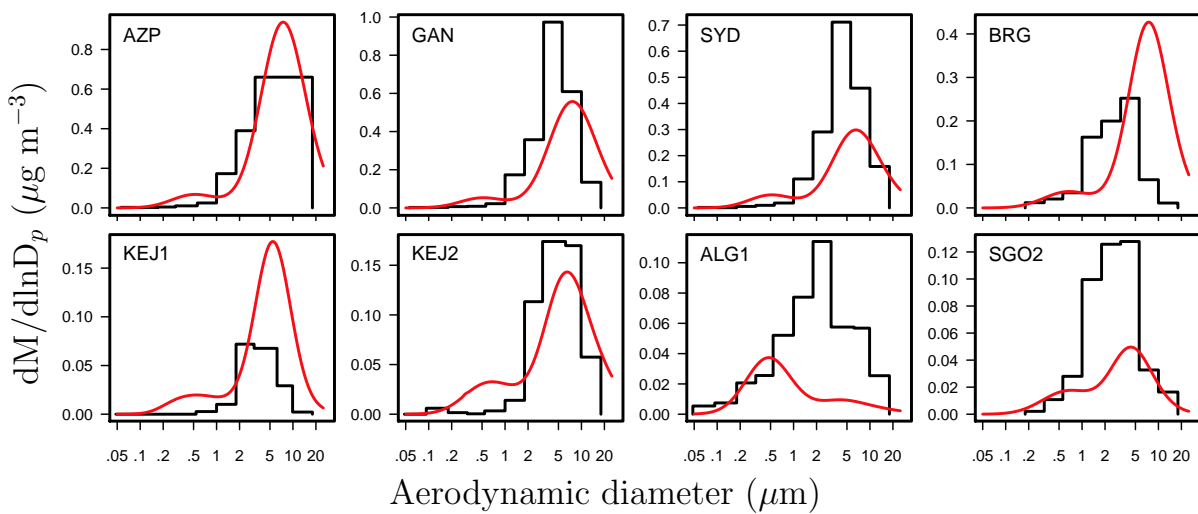


Figure 4: Average observed (black) and modeled (red) Na^+ size distributions at representative sites.

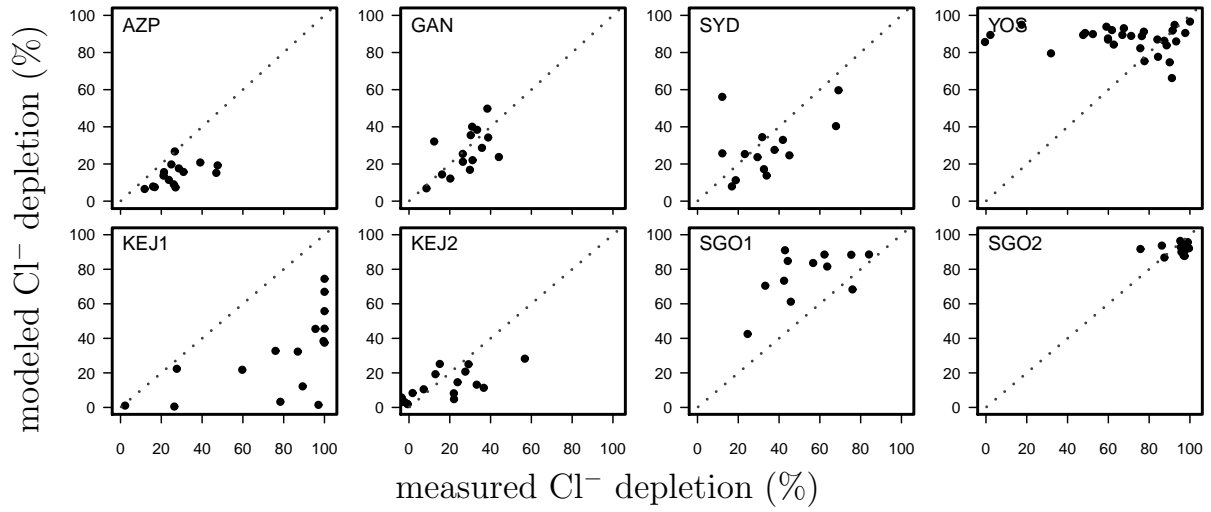


Figure 5: Scatter plots of modeled and observed chloride depletion in coarse ($D_p > 2.5\mu\text{m}$) particles at representative sites. Each point represents a distinct measurement period, with modeled concentrations averaged over the corresponding intervals.

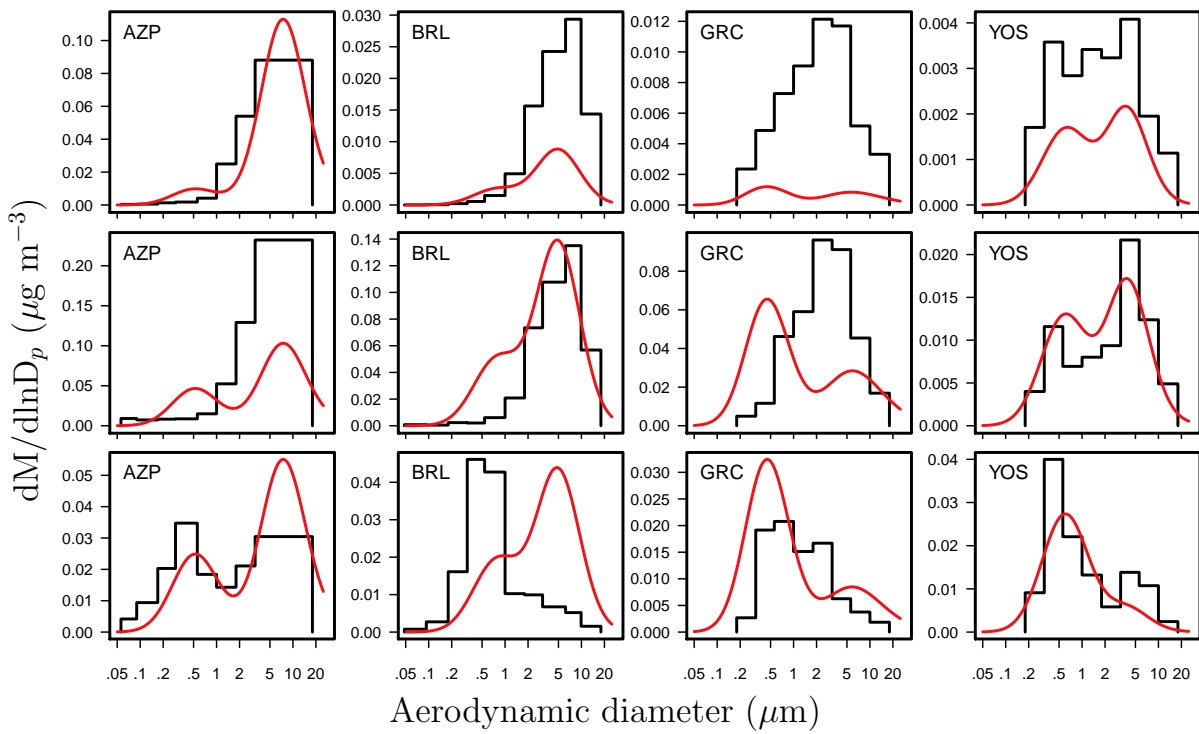


Figure 6: Average observed (black) and modeled (red) Mg^{2+} (top), Ca^{2+} (middle), and K^+ (bottom) size distributions at representative sites.

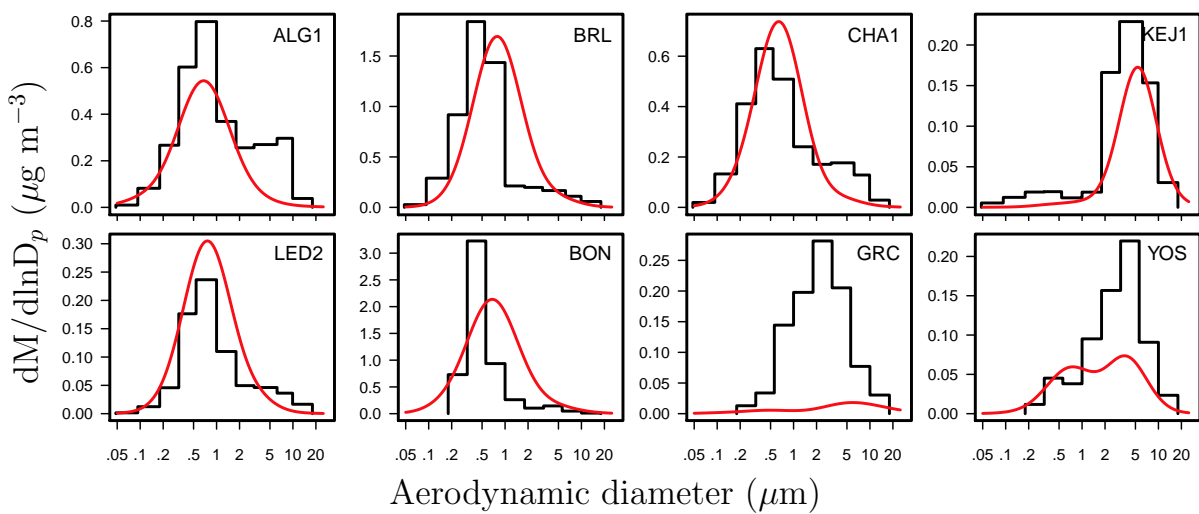


Figure 7: Average observed (black) and modeled (red) NO_3^- size distributions at representative sites.

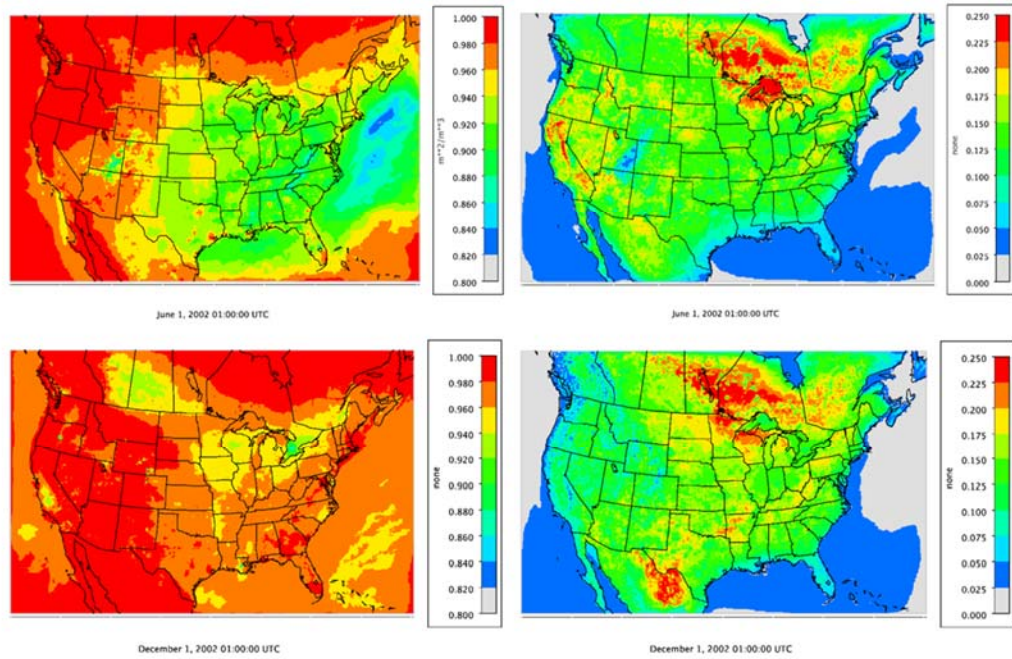


Figure 8. Fraction of accumulation mode (left) and coarse mode (right) smaller than 2.5 μm in diameter, averaged over summer (top) and winter (bottom) 2002.

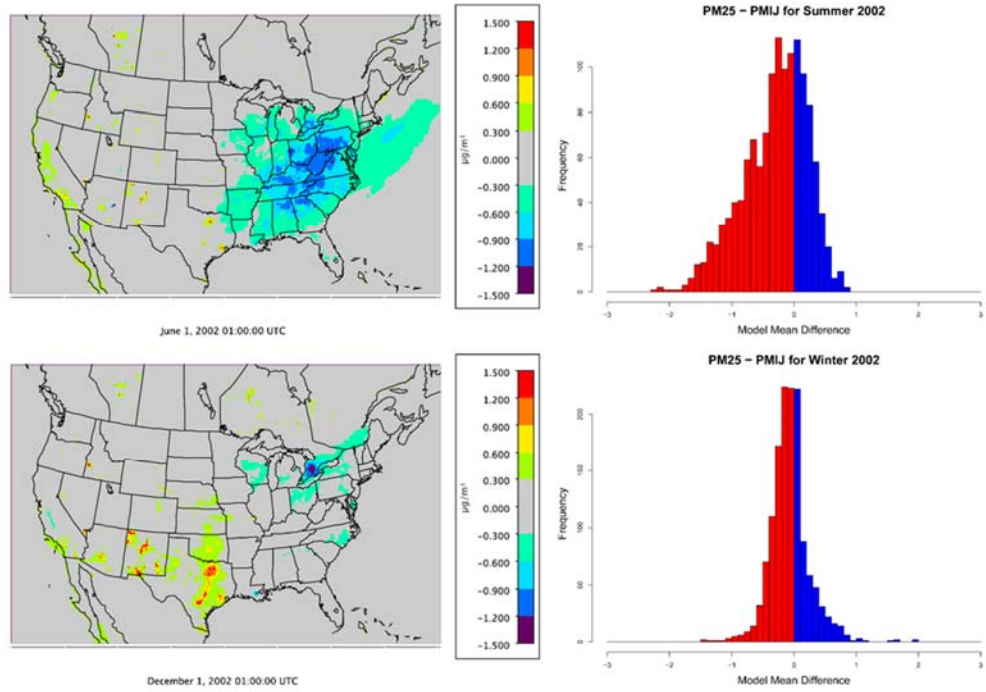


Figure 9. Difference between $\text{PM}_{2.5}$ computed using modeled size distribution and PM_{10} , and histogram of daily average $\text{PM}_{2.5} - \text{PM}_{10}$ differences for summer (top) and winter (bottom) 2002. Blue shading indicates days where $\text{PM}_{2.5}$ is greater than PM_{10} , while red shading indicates days where $\text{PM}_{2.5}$ is less than PM_{10} .

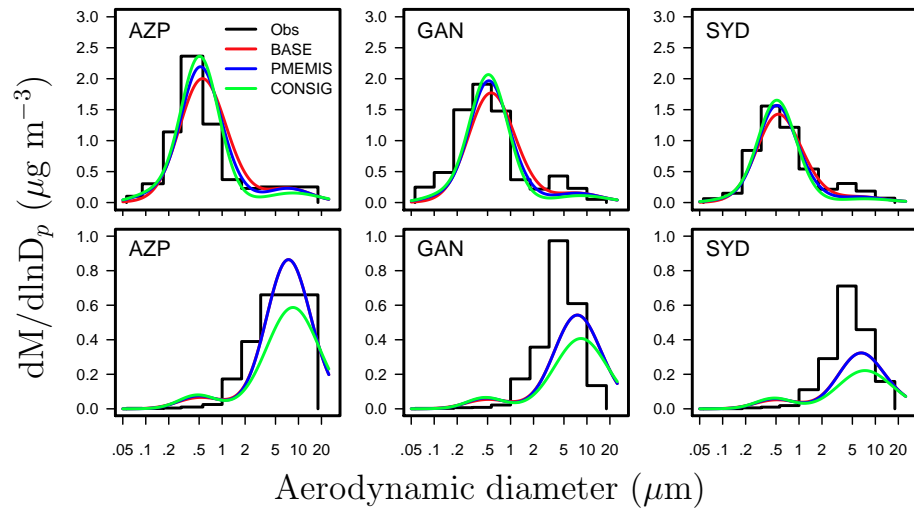


Figure 10: Observed and modeled SO_4^{2-} (top) and Na^+ (bottom) size distributions for the PMEMIS and CONSIG sensitivity simulations.

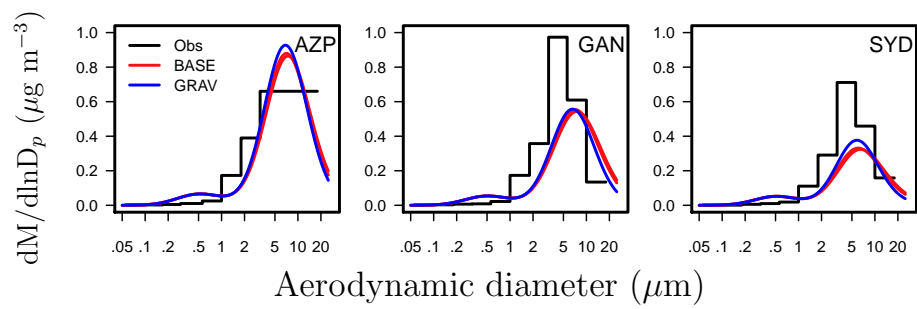


Figure 11: Observed and modeled Na^+ size distributions for the GRAV sensitivity simulation.

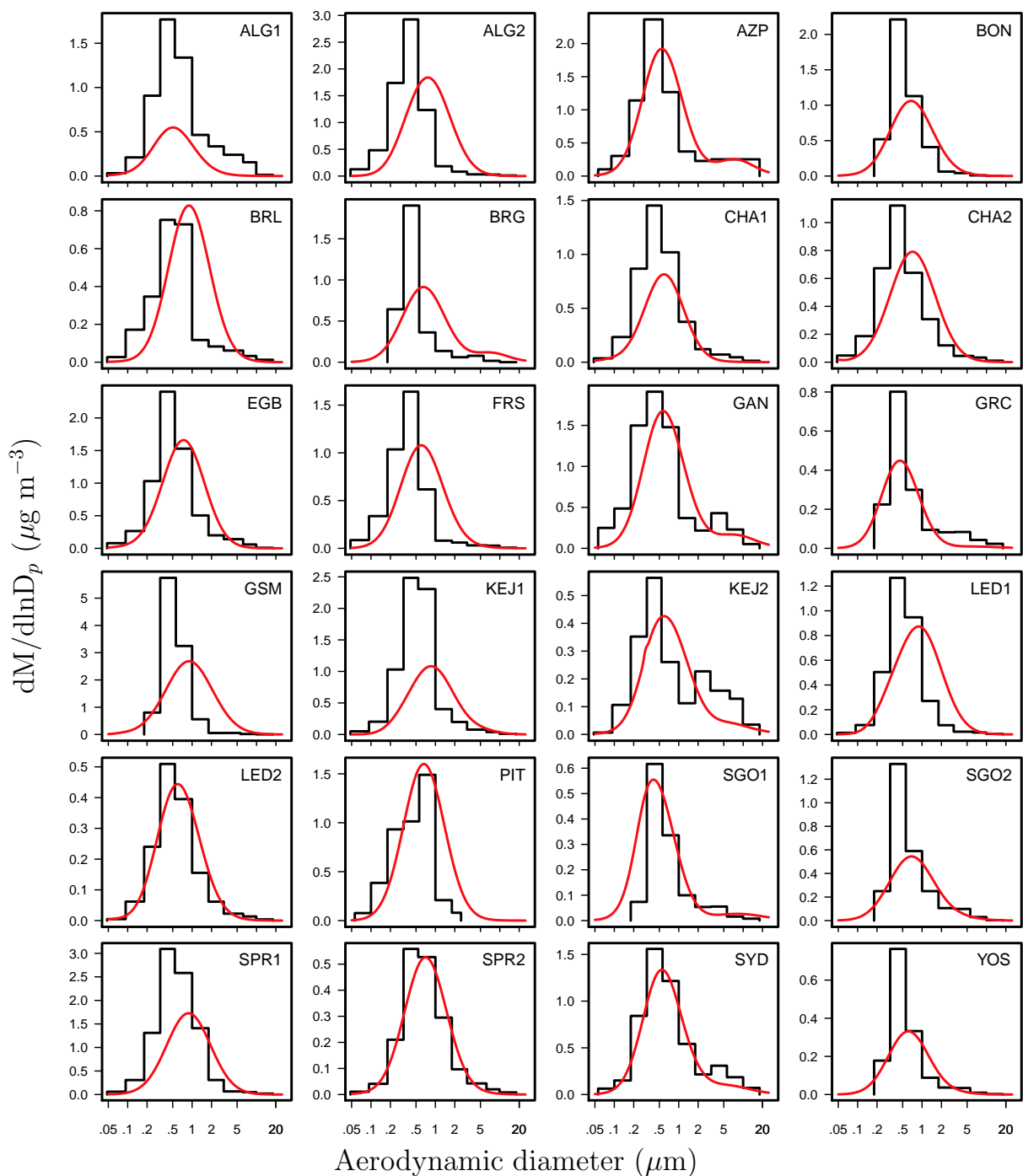


Figure S1: Average observed (black) and modeled (red) SO_4^{2-} size distributions across the 24 campaigns listed in Table 1.

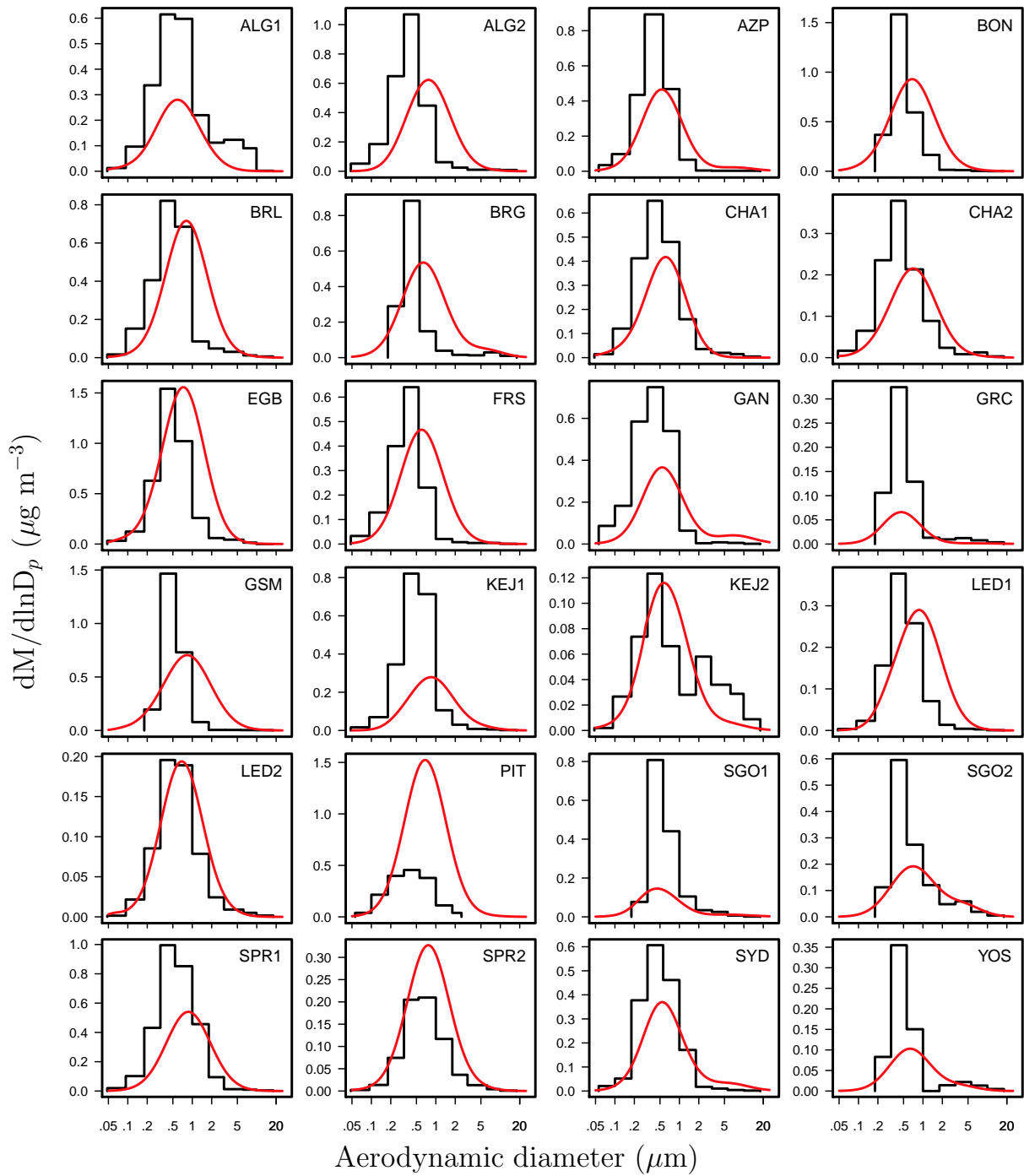


Figure S2: Average observed (black) and modeled (red) NH_4^+ size distributions across the 24 campaigns listed in Table 1.

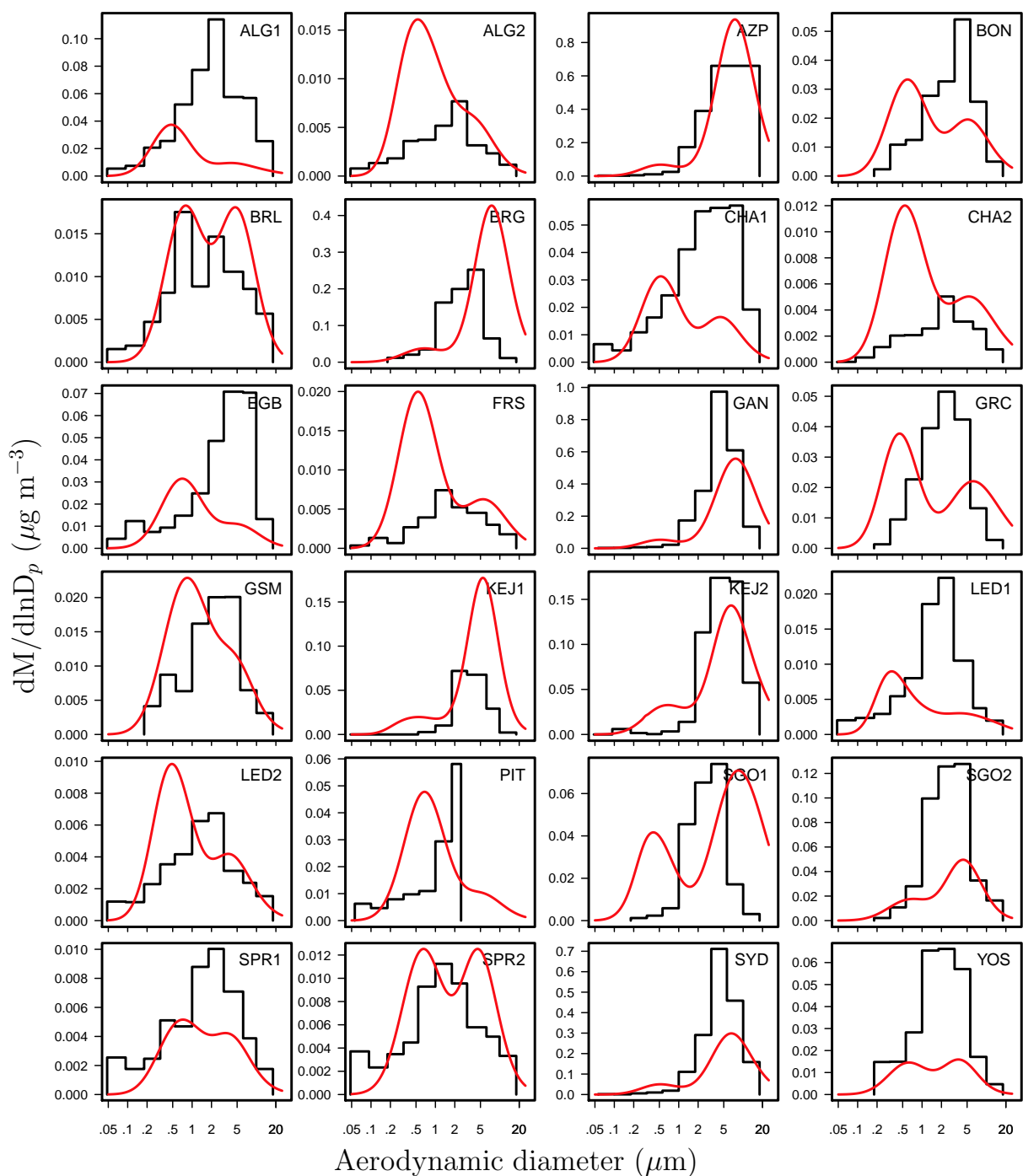


Figure S3: Average observed (black) and modeled (red) Na^+ size distributions across the 24 campaigns listed in Table 1.

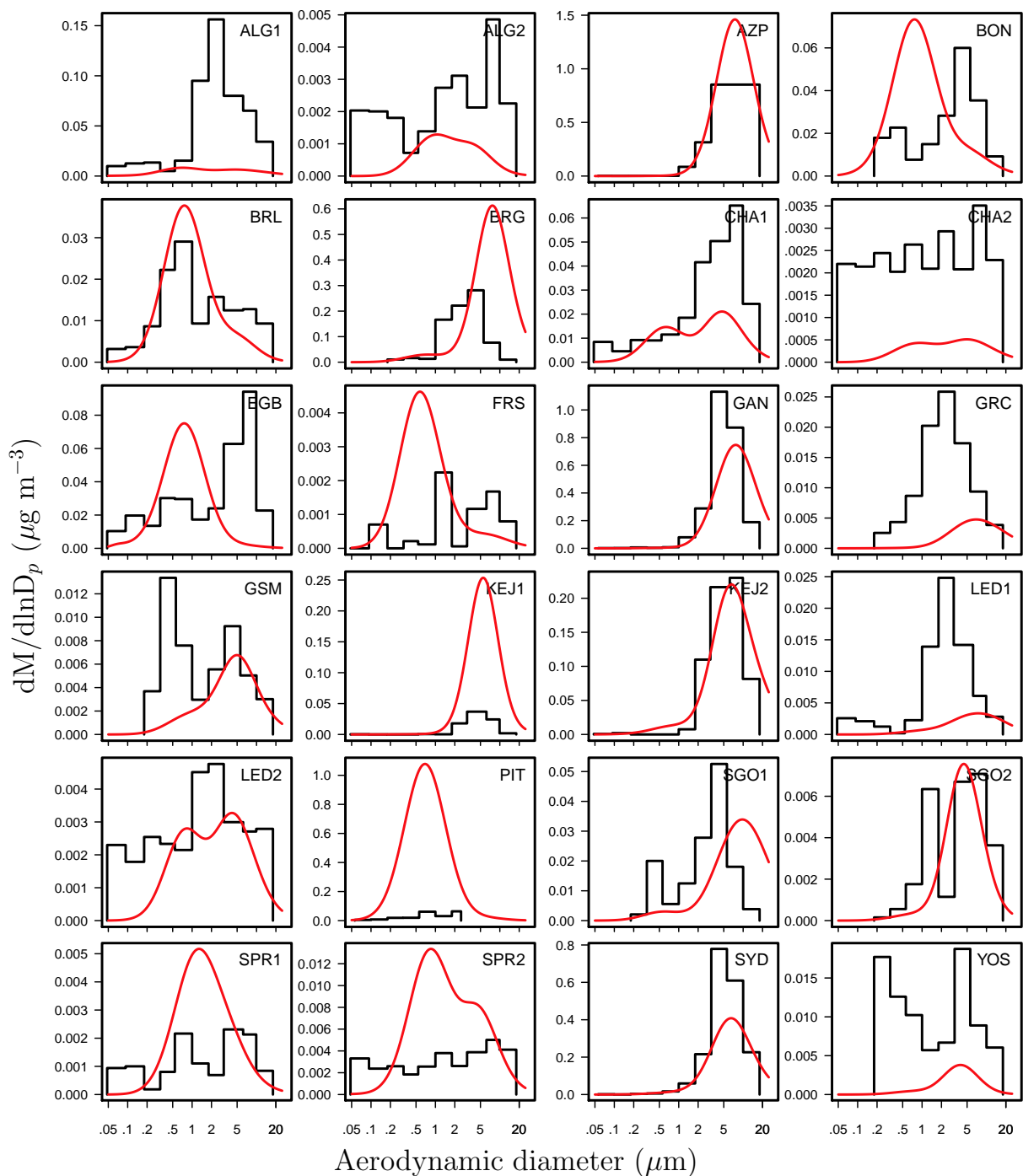


Figure S4: Average observed (black) and modeled (red) Cl^- size distributions across the 24 campaigns listed in Table 1.

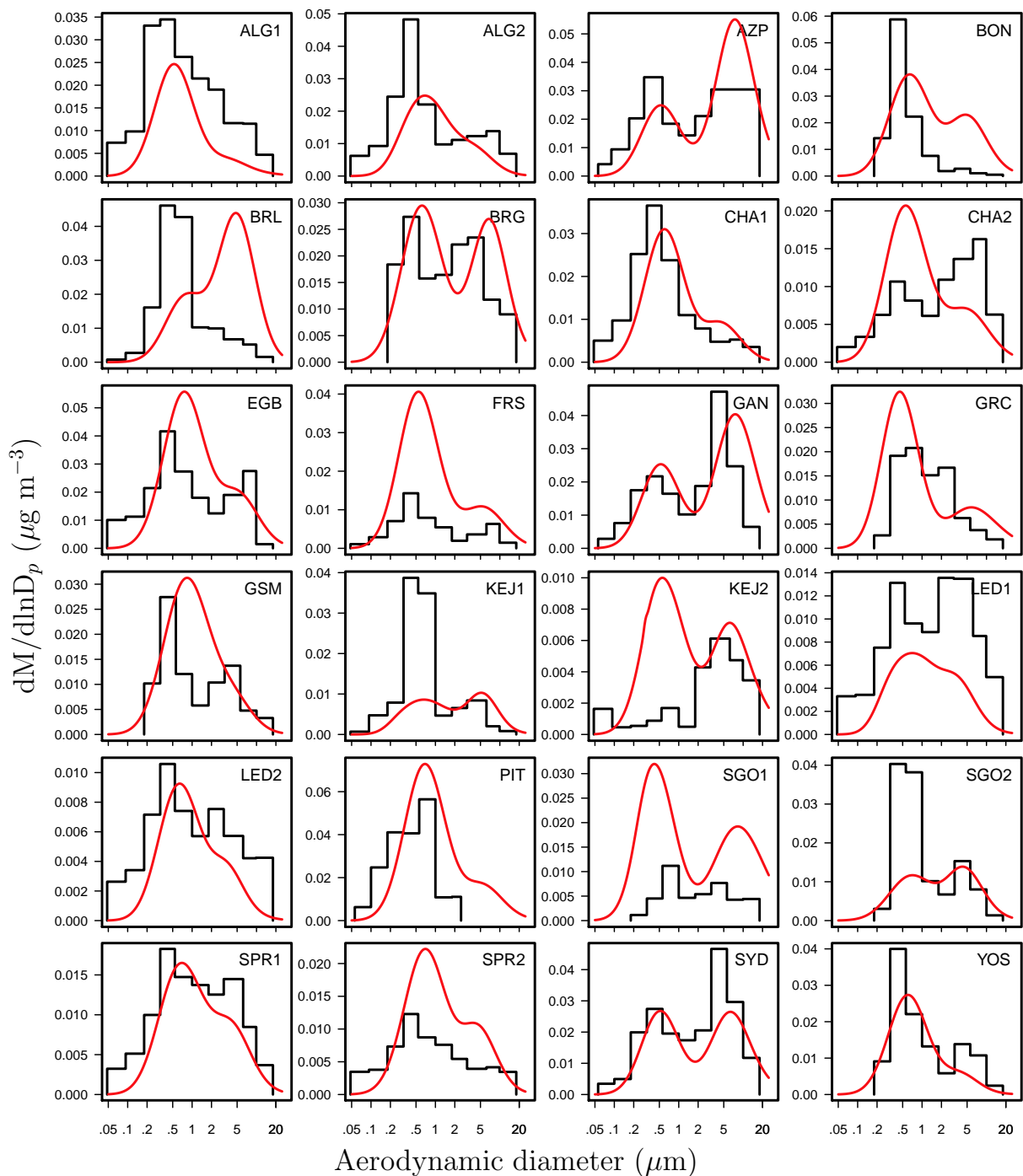


Figure S5: Average observed (black) and modeled (red) K^+ size distributions across the 24 campaigns listed in Table 1.

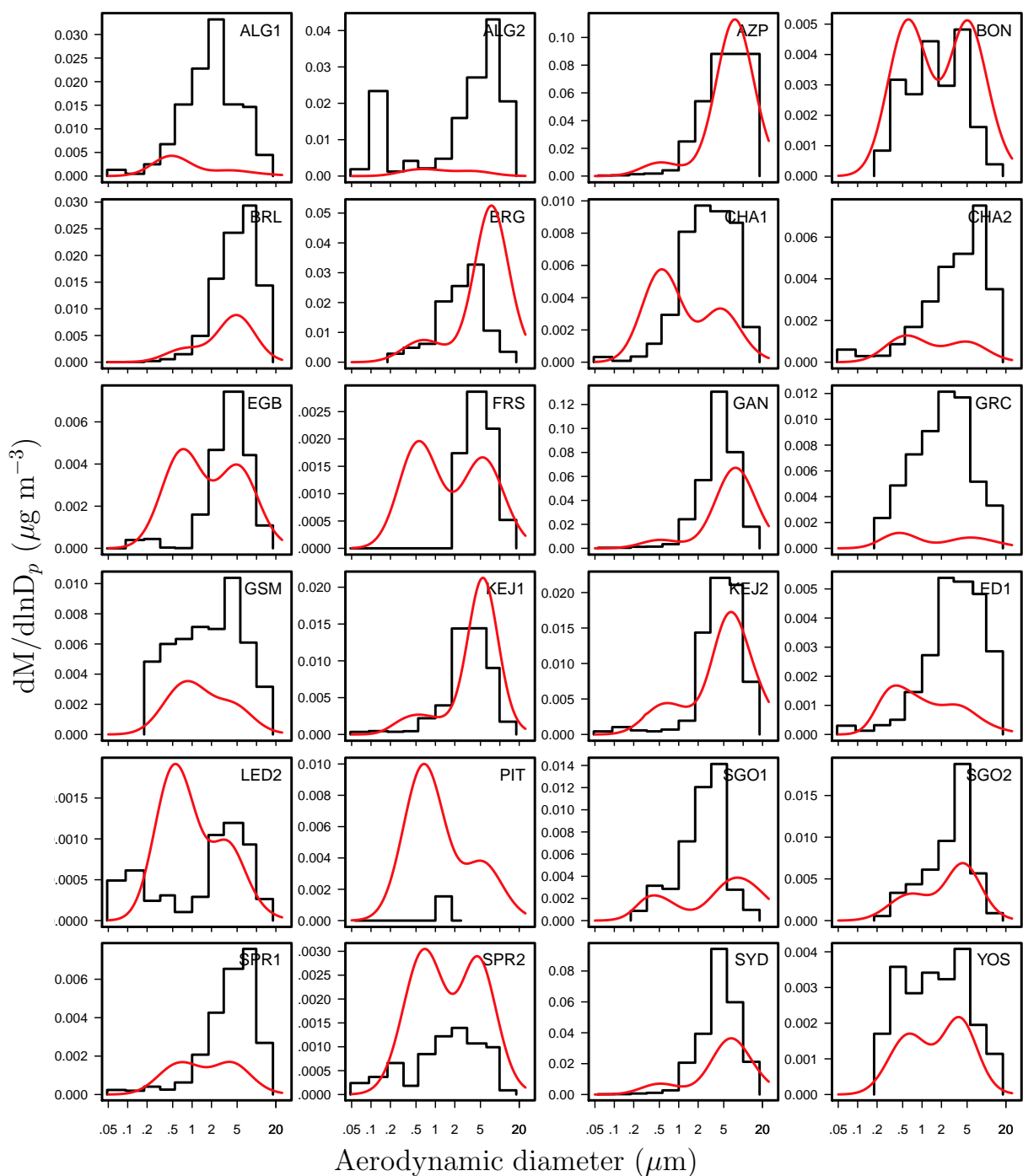


Figure S6: Average observed (black) and modeled (red) Mg^{2+} size distributions across the 24 campaigns listed in Table 1.

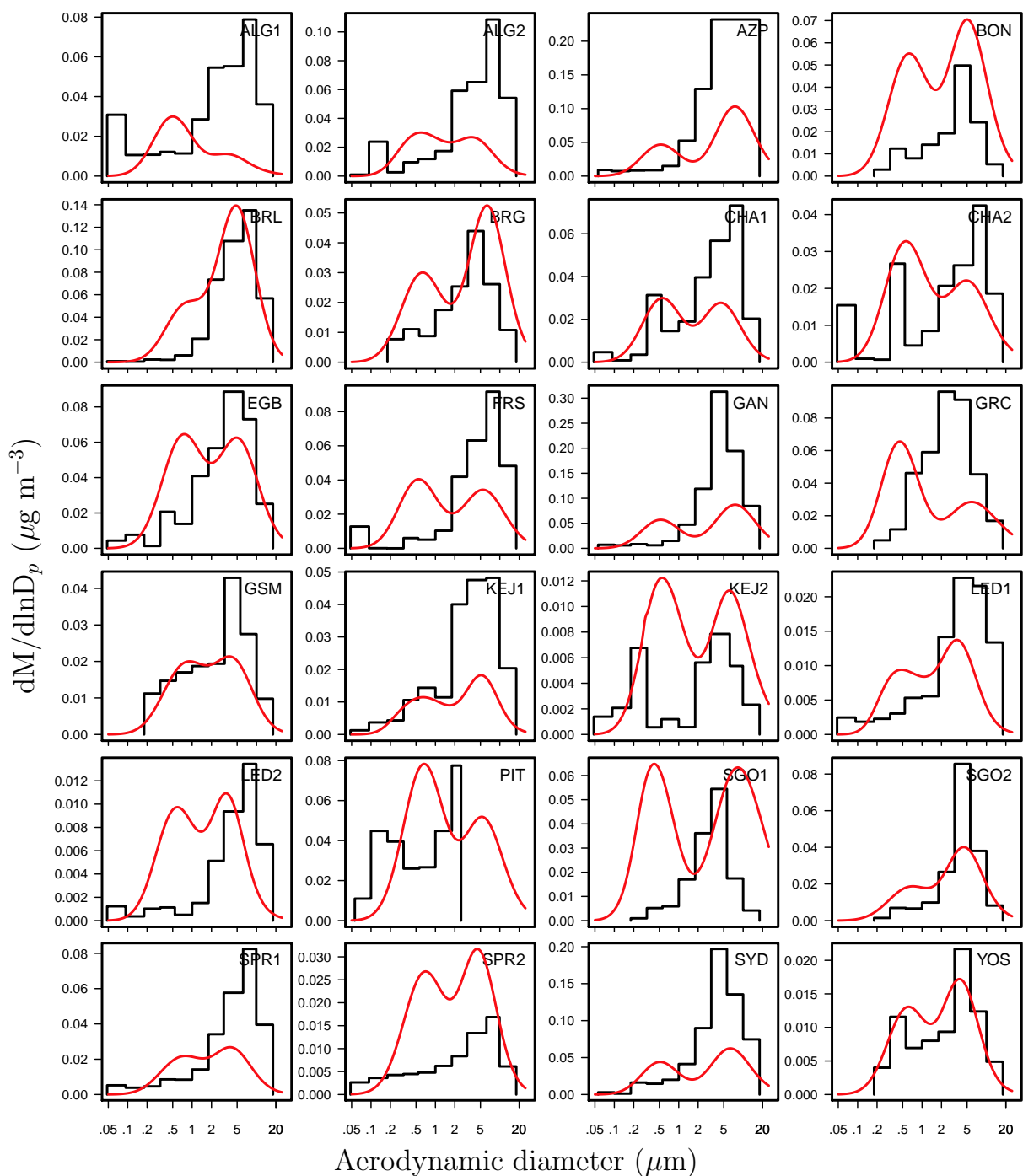


Figure S7: Average observed (black) and modeled (red) Ca^{2+} size distributions across the 24 campaigns listed in Table 1.

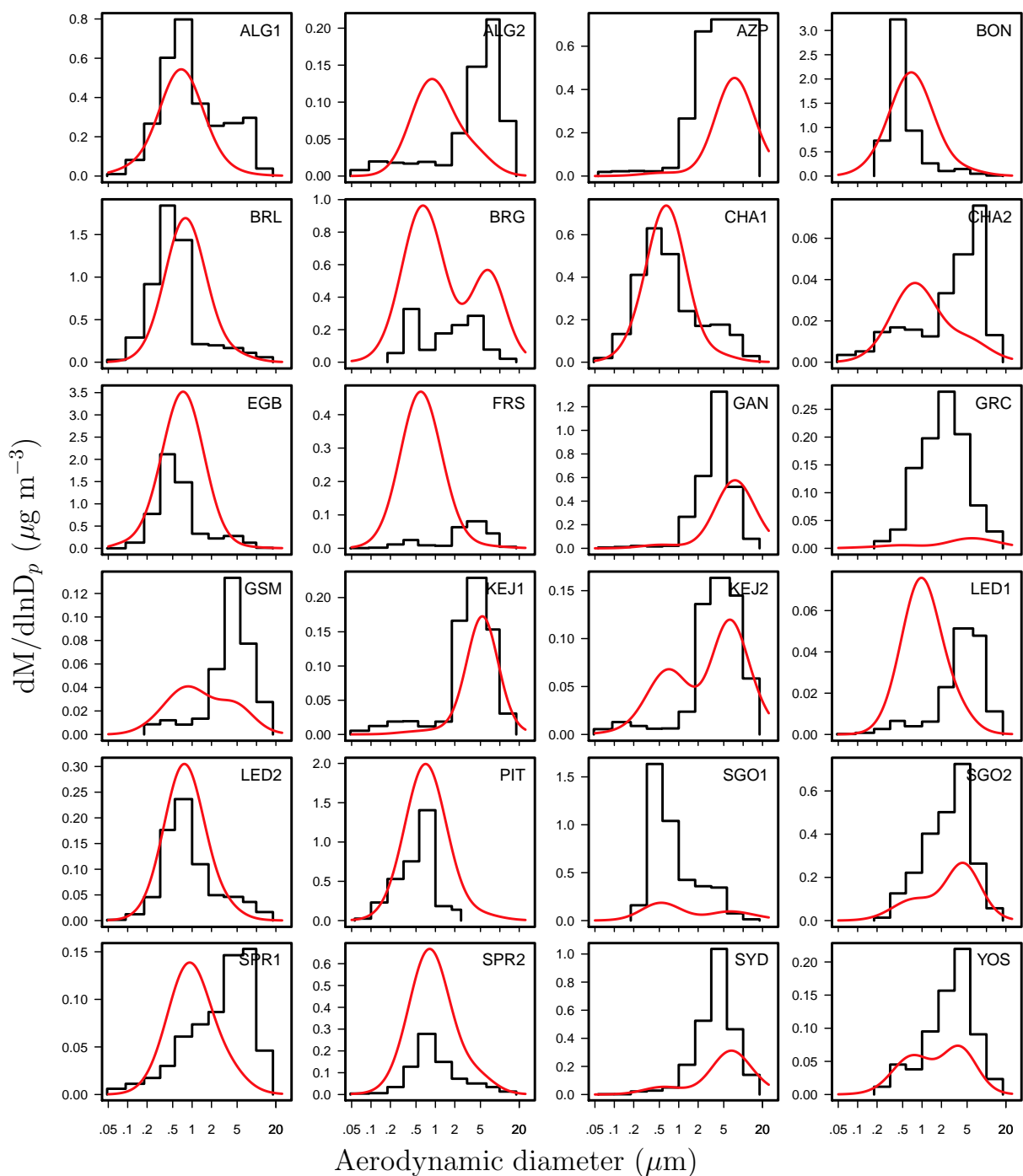


Figure S8: Average observed (black) and modeled (red) NO_3^- size distributions across the 24 campaigns listed in Table 1.

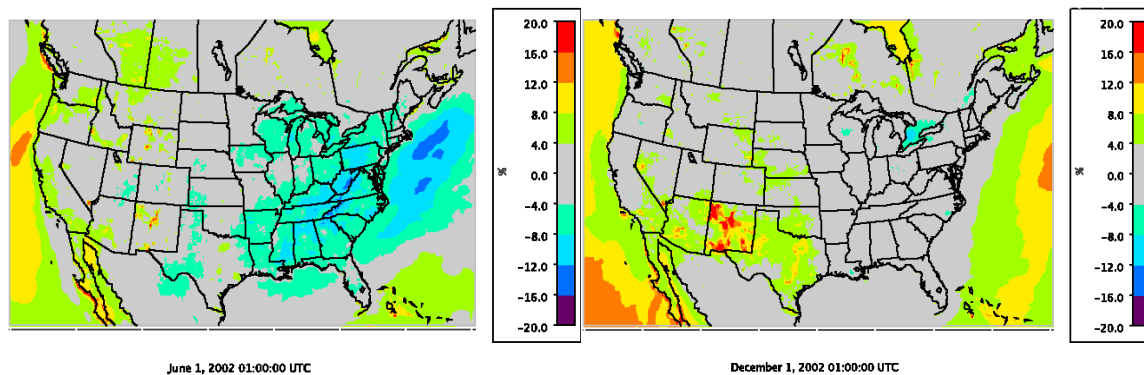


Figure S9. Mean fractional bias (%) between PM_{2.5} computed using modeled size distribution and PM₁₀, for summer (left) and winter (right) 2002.